Monthly Notices
of the
ROYAL ASTRONOMICAL SOCIETY

MNRAS **450,** 2231–2250 (2015) doi:10.1093/mnras/stv752

Modelling galaxy spectra in presence of interstellar dust – III. From nearby galaxies to the distant Universe

L. P. Cassarà,[1⋆†] L. Piovan[2,3⋆] and C. Chiosi[2⋆]

[1] *INAF-IASF Milano, Via E. Bassini 15, I-20133 Milano, Italy*
[2] *Department of Physics and Astronomy, University of Padova, Via Marzolo 8-I, I-35131 Padova, Italy*
[3] *Max-Planck-Institut für Astrophysik, Karl-Schwarzschild-Str. 1, D-85748 Garching bei München, Germany*

Accepted 2015 April 2. Received 2015 March 23; in original form 2014 November 18

ABSTRACT

Improving upon the standard evolutionary population synthesis technique, we present spectrophotometric models of galaxies with morphology going from spherical structures to discs, properly accounting for the effect of dust in the interstellar medium (ISM). The models contain three main physical components: the diffuse ISM made of gas and dust, the complexes of molecular clouds where active star formation occurs, and stars of any age and chemical composition. These models are based on robust evolutionary chemical description providing the total amount of gas and stars present at any age, and matching the properties of galaxies of different morphological types. We have considered the results obtained by Piovan et al. for the properties of the ISM, and those by Cassarà et al. for the spectral energy distribution (SED) of single stellar populations, both in presence of dust, to model the integral SEDs of galaxies of different morphological types, going from pure bulges to discs passing through a number of composite systems with different combinations of the two components. The first part of the paper is devoted to recall the technical details of the method and the basic relations driving the interaction between the physical components of the galaxy. Then, the main parameters are examined and their effects on the SED of three prototype galaxies are highlighted. The theoretical SEDs nicely match the observational ones both for nearby galaxies and those at high redshift.

Key words: radiative transfer – dust, extinction – galaxies: bulges – galaxies: evolution – galaxies: formation.

1 INTRODUCTION

In recent years, the first epoch of galaxy formation has been continuously pushed back in time by the discovery of galaxy size objects at higher and higher redshifts, $z \sim 4$–5 (Madau et al. 1996; Steidel et al. 1999), $z \sim 6$ (Stanway, Bunker & McMahon 2003; Dickinson et al. 2004) to $z \sim 10$ (Bouwens et al. 2014; Oesch et al. 2012; Zheng et al. 2012), up to $z \sim 10$–20 according to the current view (Rowan-Robinson 2012). Furthermore, this high-redshift Universe turned out to be heavily obscured by copious amounts of dust (see for instance, Carilli et al. 2001; Shapley et al. 2001; Robson et al. 2004; Wang et al. 2009; Michałowski et al. 2010), whose origin and composition are a matter of vivid debate (Draine 2009; Dwek, Galliano & Jones 2009; Dwek & Cherchneff 2011; Gall, Andersen & Hjorth 2011a,b). In this context, the current paradigm is that the interstellar dust plays an important role in galaxy formation and evolution. Therefore, understanding the properties of this interstellar dust and setting a physically realistic interplay between populations of stars and dust are critical to determine the properties of the high-z Universe and to obtain precious clues on the fundamental question about when and how galaxies formed and evolved.

It follows from all this that to fully exploit modern data, realistic spectrophotometric models of galaxies must include the important component of the interstellar medium (ISM). This has spurred unprecedented effort in the theoretical modelling of the spectrophotometry, dynamics, and chemistry of dusty galaxies (see for instance, Jonsson, Groves & Cox 2010; Narayanan et al. 2010; Grassi et al. 2011; Pipino et al. 2011; Popescu et al. 2011). Dust absorbs the stellar radiation and re-emits it at longer wavelengths, deeply changing the shape of the observed spectral energy distributions (SEDs; Silva et al. 1998; Piovan, Tantalo & Chiosi 2006b; Popescu et al. 2011). It also strongly affects the production of molecular hydrogen and the local amount of ultraviolet (UV) radiation in galaxies, playing a strong role in the star formation process (Yamasawa et al. 2011).

⋆E-mail: letizia.cassara@gmail.com (LPC); lorenzo.piovan@gmail.com (LP); cesare.chiosi@unipd.it (CC)
†Present address: National Observatory of Athens – Institute for Astronomy, Astrophysics, Space Applications & Remote Sensing, Vas. Pavlou & I. Metaxa, 15236 Penteli, Greece.

This paper is a sequel of the series initiated with Piovan, Tantalo & Chiosi (2003, 2006a) and Piovan et al. (2006b) devoted to modelling the spectra of galaxies of different morphological type in presence of dust. In this paper, we present new results for the light emitted by galaxies of different morphological type and age. Our galaxy model contains three interacting components: the diffuse ISM, made of gas and dust, the large complexes of molecular clouds (MCs) in which active star formation occurs, and, finally, the populations of stars that are no longer embedded in the dusty environment of their parental MCs. Furthermore, our model for the dust takes into account three components, i.e. graphite, silicates, and polycyclic aromatic hydrocarbons (PAHs). We consider and adapt to our aims two prescriptions for the size distribution of the dust grains and two models for the emission of the dusty ISM. The final model we have adopted is a hybrid one which stems from combining the analysis of Guhathakurta & Draine (1989) for the emission of graphite and silicates and Puget, Leger & Boulanger (1985) for the PAH emission, and using the distribution law of Weingartner & Draine (2001b) and the ionization model for PAHs of Weingartner & Draine (2001a). The SEDs of single stellar populations (SSPs) of different age and chemical composition, the building blocks of galactic spectra, are taken from Cassarà et al. (2013) who have revised the contribution by asymptotic giant branch (AGB) stars taking into account new models of stars in this phase by Weiss & Ferguson (2009) and include the effect of dust on both young stars and AGB stars. During the history of an SSP, there are two periods of time in which self-obscuration by dust in a cloud surrounding a star plays an important role, causing internal absorption and re-emission of the light emitted by central object: when young massive stars are still embedded in their parental MCs and when intermediate- and low-mass AGB stars are forming their own dust shell (see Piovan et al. 2003, 2006a,b; Cassarà et al. 2013, for more details about AGB stars). With the aid of all this, we seek to get clues on the spectrophotometric evolution of galaxies, in particular taking into account the key role played by dust in determining the spectrophotometric properties of the stellar populations, and to set up a library of template model galaxies of different morphological type (from pure spheroids to pure discs and intermediate types with the two components in different proportions) whose SEDs at different evolutionary times can be compared with galaxies of the Local Universe and as function of redshift.

The strategy of the paper is as follows. The model we have adopted is shortly summarized in Section 2 where first we define the galaxy components we are dealing with, i.e. bare stars, stars embedded in MC complexes, and diffuse ISM; secondly, we outline the recipes and basic equations for the gas infall, chemical evolution, initial mass function (IMF), and star formation rate (SFR); thirdly, we describe how the total amounts of stars, MCs, and ISM present in the galaxy at a certain age are distributed over the galaxy volume by means of suitable density profiles, one for each component depending on the galaxy type: pure disc galaxies, pure spheroidal galaxies, and composite galaxies with both disc and bulge; finally, the galaxy volume is split in suitable elemental volumes to each of which the appropriate amounts of stars, MCs, and ISM are assigned. In Section 3, we explain how the SEDs of galaxies of different morphological type are calculated in presence of the dust in the ISM. First, the technical details of the method are described and basic relationships/equations describing the interaction between the physical components of the galaxy are presented. In Section 4, we shortly describe the composition of the dust. In Section 5, we list and discuss the key parameters of the chemical and spectrophotometric models for the three basic types of galaxy: pure discs, pure spheroids, and composite systems. In Section 6, the SED of a few proto-type galaxies are presented, first as it would be observed at the present time and then as a function of the age. In Section 7, we examine the present-day theoretical colours in widely used photometric systems as a function of the morphological type of the underlying galaxy and compare them with literature data. In Section 8, we present the colour evolution of the model galaxies as a function of redshift assuming the nowadays most credited Λ cold dark matter (ΛCDM) cosmological scenario and compare the theoretical colours with the observational data currently available in literature. Finally, some concluding remarks are drawn in Section 9.

2 MODELS OF GALAXIES OF DIFFERENT MORPHOLOGICAL TYPES

2.1 Physical components of galaxy models

As originally proposed by Silva et al. (1998) and then adopted in many evolutionary population synthesis (EPS) models with dust (see for instance, Bressan, Silva & Granato 2002; Piovan et al. 2006a,b; Galliano, Dwek & Chanial 2008; Popescu et al. 2011), the most refined galaxy models with dust available in literature contain three physical components.

(i) The diffuse ISM, composed by gas and dust; the model for the ISM adopted in this study is described in detail in Piovan et al. (2006a) and includes a state-of-art description of a three-component ISM made by graphite, silicates, and PAHs, the most widely adopted scheme for a dusty ISM.

(ii) The large complexes of MCs where active star formation takes place. In our model, we do not consider H II regions and nebular emission. The MCs hide very young stars; their SEDs are severely affected by the dusty environment around them and skewed towards the IR. The library of dusty MCs for which a ray-tracing radiative transfer code has been adopted is presented in Piovan et al. (2006a) at varying the input parameters.

(iii) The populations of stars free from their parental MCs. They are both intermediate-age AGB stars (with age from about 0.1 to 1–2 Gyr) that are intrinsically obscured by their own dust shells (Piovan et al. 2003; Marigo et al. 2008), and the old stars that shine as bare objects and whose radiation propagates through the diffuse galactic ISM. The effect of dust around AGB stars has been included ex novo taking into account the new models of TP-AGB stars by Weiss & Ferguson (2009) as described in Cassarà et al. (2013), where new SEDs of SSPs have been presented and tested.

The models of galaxies are based on a robust evolutionary chemical model that, considering a detailed description for the gas infall, star formation law, IMF, and stellar ejecta, provides the total amount of gas and stars present at any age, with their chemical history (Chiosi 1980; Tantalo et al. 1996, 1998; Portinari, Chiosi & Bressan 1998; Portinari & Chiosi 1999, 2000; Piovan, Tantalo & Chiosi 2006b). These chemical models are adjusted in order to match the gross properties of galaxies of different morphological type. The interaction between stars and ISM in building up the total SED of a galaxy is described using a suitable spatial distribution of gas and stars. For each type of galaxies, a simple geometrical model is assumed. The following step is to distribute the total gas and star mass provided by the chemical model over the whole volume, using suitable density profiles, according to each component and depending on the galaxy type (pure spheroid, pure disc, and a combination of disc plus bulge). The galaxy is split in suitable volume elements; each elemental volume contains the appropriate

amounts of stars, MCs, and ISM and it is at the same time source of radiation (from the stars inside) and absorber and emitter of radiation (from and to all other elemental volumes and the ISM in between). These elements are the primordial seeds to calculate the global galaxy SED.

2.2 The star formation and chemical enrichment of galaxy models

The so-called *infall-model*, developed by Chiosi (1980), and used by many authors [Bressan, Chiosi & Fagotto (1994), Tantalo et al. (1996), Tantalo et al. (1998), Portinari et al. (1998)] characterizes the star formation and chemical enrichment histories of the model galaxies. Originally conceived for disc galaxies, over the years it has been also extended to early-type galaxies (ETGs). In this paragraph, the main features of the infall model are presented.

Within a halo of arbitrary shape and volume, which contains dark matter (DM) of mass $M_{\rm DM}$, the mass of the baryonic (luminous) matter, $M_{\rm BM}$, evolves with time by infall of primordial gas following the law

$$\frac{{\rm d}M_{\rm BM}\,(t)}{{\rm d}t} = M^0_{\rm BM} \exp\left(-\frac{t}{\tau}\right), \tag{1}$$

where τ is the infall time-scale. The constant $M^0_{\rm BM}$ is fixed considering that at the present age $t_{\rm G}$ the mass $M_{\rm BM}(t)$ is equal to $M_{\rm BM}(t_{\rm G})$. The baryonic (luminous) asymptotic mass of the galaxy becomes

$$M^0_{\rm BM} = \frac{M_{\rm BM}\,(t_{\rm G})}{\tau[1-{\rm e}^{(-t_{\rm G}/\tau)}]} \tag{2}$$

while the time variation of the BM is

$$M_{\rm BM}\,(t) = \frac{M_{\rm BM}\,(t_{\rm G})}{\tau[1-{\rm e}^{(-t_{\rm G}/\tau)}]}[1-{\rm e}^{(-t/\tau)}]. \tag{3}$$

For more details, we refer to Tantalo et al. (1996, 1998).

2.2.1 *ETGs and/or bulges*

Applied to an ETG or a bulge, our infall model of chemical evolution can *mimic* the collapse of the parental proto-galaxy made of BM and DM in cosmological proportions from a very extended size to the one we see today. Under self-gravity, both DM and BM collapse and shrink at a suitable rate. As the gas falls and cools down into the common potential well, the gas density increases so that star formation begins. A central visible object is formed. Soon or later, both components virialize and settle to an equilibrium condition, whose geometrical shape is close to a sphere. In this case, the galaxy can be approximated by a sphere of DM with mass $M_{\rm DM}$ and radius $R_{\rm DM}$, containing inside a luminous, spherical object of mass $M_{\rm BM}$ and radius $R_{\rm BM}$. As more gas flows in, the star formation becomes more efficient. Eventually, the whole gas content is exhausted and turned into stars, thus quenching further star formation. At the beginning, the SFR is small, then rises to a maximum, and subsequently it declines. Because of the more efficient chemical enrichment of the infall model, the initial metallicity for the bulk of star-forming activity is significantly different from zero. The radius of the stellar component of a galaxy will grow with its mass according to the law of virial equilibrium. It must be underlined that the collapse of the proto-galactic cloud cannot be modelled in a realistic dynamical way using a traditional chemical code: to simulate the gas dynamics, another technique must be used (see for instance, Chiosi & Carraro 2002; Springel, Di Matteo & Hernquist 2005; Gibson et al. 2007; Merlin & Chiosi 2007; Merlin et al. 2010, 2012). However, these models require lots of computational time and do not allow us to quickly explore the parameter space. Therefore, our chemical model will be a *static* one simulating the formation of the galaxy by the collapse of primordial gas in presence of DM in a simple fashion. In other words, the model galaxy is conceived as a mass point (Chiosi 1980) for which no information about the spatial distribution of stars and gas is available. These will be distributed according to suitable prescriptions (see below where the distribution laws and the normalization of the physical quantities are explained in detail for the different morphological types). Finally, it is worth recalling that the chemical history of spheroidal systems is best described by models in which galactic winds can occur.

2.2.2 *Disc galaxies*

In the case of pure disc galaxies or of the disc component of intermediate-type galaxies, it is reasonable to assume that discs are the result of accumulation of primordial or partially enriched gas at a suitable rate (as originally suggested by the dynamical studies of Larson 1976; Burkert, Truran & Hensler 1992). If so, the formalism presented above can be extended to model galactic discs, provided we identify the baryonic mass $M_{\rm BM}(t)$ with the surface mass density and consider the disc as made by a number of isolated and independent concentric rings in which the mass grows as a function of time (Portinari & Chiosi 1999, 2000) or as a number of rings in mutual communication thanks to radial flows of gas and dust (Portinari & Chiosi 2000). However, for the purposes of this study the simple one-zone formulation is fully adequate also for disc galaxies: the radial dependence is left aside and the disc is modelled as a dimensionless object as in the classical paper by Talbot & Arnett (1971). This simple model well reproduces the results of dynamical models (Larson 1976; Burkert et al. 1992; Carraro, Ng & Portinari 1998), with the exception of the radial flows of gas. As for the spheroidal objects above, the spatial distribution of stars and gas in the disc will be introduced by hand later on (see below). The chemical history and dynamical structure of galactic discs are fully compatible with absence of galactic winds that are found not to play a significant role. The argument is based on the high temperature in the disc–halo interface needed for thermal winds as thoroughly discussed by Breitschwerdt & Komossa (2000) and Spitoni, Matteucci & Marcon-Uchida (2013) to whom we refer for all details.

2.2.3 *Gravitational potential of a spherical system and galactic wind*

In order to determine the physical conditions under which galactic winds may occur, we need to evaluate the gravitational potential of spherical systems made of DM and BM with different radial distributions. In the following, we adopt the formalism developed by Tantalo et al. (1996) that is shortly summarized here for the sake of clarity. The spatial distribution of DM with respect to BM follows the dynamical models of Bertin, Saglia & Stiavelli (1992) and Saglia, Bertin & Stiavelli (1992): the mass and radius of the DM (M_{DM} and R_{DM}) are linked to those of the BM ($M_{\rm BM}$ and $R_{\rm BM}$) by

$$\frac{M_{\rm BM}(t)}{M_{\rm DM}} \geq \frac{1}{2\pi}\left(\frac{R_{\rm BM}(t)}{R_{\rm DM}}\right)\left[1+1.37\left(\frac{R_{\rm BM}(t)}{R_{\rm DM}}\right)\right]. \tag{4}$$

The mass of the dark component is supposed to be constant in time and equal to $M_{\rm DM} = \beta M_{\rm BM}(t_{\rm G})$, where $M_{\rm BM}(t_{\rm G})$ is the asymptotic content of BM of a galaxy, and $\beta \simeq 6$ is given by the baryon ratio

in the ΛCDM Universe we have adopted (Hinshaw et al. 2009). With these assumptions, the binding gravitational energy of the gas is given by

$$\Omega_{\rm g}(t) = -\alpha_{\rm BM} G \frac{M_{\rm g}(t) M_{\rm BM}(t)}{R_{\rm BM}(t)} - G \frac{M_{\rm g}(t) M_{\rm DM}}{R_{\rm BM}(t)} \Omega'_{\rm BD}, \quad (5)$$

where $M_{\rm g}(t)$ is the current value of the gas mass, $\alpha_{\rm BM}$ is a numerical factor $\simeq 0.5$, while

$$\Omega'_{\rm BD} = \frac{1}{2\pi} \left(\frac{R_{\rm BM}(t)}{R_{\rm DM}} \right) \left[1 + 1.37 \left(\frac{R_{\rm BM}(t)}{R_{\rm DM}} \right) \right] \quad (6)$$

is the contribution to the gravitational energy given by the presence of DM. Adapting the original assumptions by Bertin et al. (1992) and Saglia et al. (1992) to the present situation, we assume $M_{\rm BM}/M_{\rm DM} = 0.16$ and $R_{\rm BM}/R_{\rm DM} = 0.16$. Using these values for $M_{\rm BM}/M_{\rm DM}$ and $R_{\rm BM}/R_{\rm DM}$, the contribution to gravitational energy by the DM is $\Omega'_{\rm BD} = 0.03$. Assuming that at each stage of the infall process the amount of luminous mass that has already accumulated gets soon virialized and turned into stars, the total gravitational energy and radius of the material already settled in the equilibrium configuration can be approximated by the relation between the total gravitational energy and the radius as a function of mass (Saito 1979a,b): for elliptical galaxies, the spatial distribution of stars is such that the global luminosity profile follows the $R^{1/4}$ law. The relation between $R_{\rm BM}(t)$ and $M_{\rm BM}(t)$ becomes

$$R_{\rm BM}(t) = 26.1 \times (M_{\rm BM}(t)/10^{12} {\rm M}_\odot)^{(2-\eta)} \ {\rm kpc} \quad (7)$$

with $\eta = 1.45$ (see Arimoto & Yoshii 1987; Tantalo et al. 1998).

If DM and BM are supposed to have the same spatial distribution, equations (5) and (6) are not needed: the binding energy becomes

$$\Omega_{\rm g}(t) = \Omega_{\rm L+D}(t) M_{\rm g}(t) [2 - M_{\rm g}(t)]. \quad (8)$$

In spheroidal systems, the *galactic wind* is supposed to occur when the thermal energy of the gas in the galaxy, heated by the SNe explosions, by stellar winds, and by UV radiation from massive stars and cooled down by radiative processes, equals or exceeds the gravitational potential energy

$$E_{\rm th,g}(t) \geq \Omega_{\rm g}(t). \quad (9)$$

The star formation is hence quenched and all the remaining gas is expelled. In contrast, no galactic winds are supposed to occur in disc galaxies.

2.2.4 Basic chemical equations

The complete formalism of the chemical evolution models providing the backbone of the photometric history of galaxies can be found in Tantalo et al. (1996) for a spherical system and in Portinari & Chiosi (2000) for disc galaxies with radial flows [see also Cassarà (2012) for an exhaustive review of the various models in the literature]. Here, we show only the final equations for the chemical evolution of an ISM made of dust and gas lumped together in a single component.

Indicating with $M_{\rm g}(t)$ the mass of gas at the time t, the corresponding gas fraction is

$$G(t) = \frac{M_{\rm g}(t)}{M_{\rm B}(t_{\rm G})}.$$

Denoting with $X_i(t)$ the mass abundance of the ith chemical species, we may write

$$G_i(t) = X_i(t) G(t),$$

where by definition $\sum_i X_i = 1$.

The evolution of the normalized masses G_i and abundances $X(i)$ of the ith element is given by the following system of equations:

$$\begin{aligned} \frac{\rm d}{{\rm d}t} G_i(t) = & -X_i(t) \psi(t) \\ & + \int_0^{t-\tau_{M_{\rm b,l}}} \psi(t') \left[R_{\phi(M)} \right]_{M(t-t')} {\rm d}t' \\ & + (1-A) \int_{t-\tau_{M_{\rm b,l}}}^{t-\tau_{M_{\rm b,u}}} \psi(t') \left[R_{\phi(M)} \right]_{M(t-t')} {\rm d}t' \\ & + \int_{t-\tau_{M_{\rm b,u}}}^{t-\tau_{M_{\rm u}}} \psi(t') \left[R_{\phi(M)} \right]_{M(t-t')} {\rm d}t' \\ & + A \int_{t-\tau_{M_{1,\max}}}^{t-\tau_{M_{1,\min}}} \psi(t') \left[R_{f(M_1)} \right]_{M_1(t-t')} {\rm d}t' \\ & + R_{\rm SNI} E_{{\rm SNI},i} \\ & + \left[\frac{\rm d}{{\rm d}t} G_i(t) \right]_{\rm inf} - \left[\frac{\rm d}{{\rm d}t} G_i(t) \right]_{\rm out}, \end{aligned} \quad (10)$$

where

$$\left[R_{\phi(M)} \right]_{M(t-t')} = \left[\phi(M) R_i(M) \left(-\frac{{\rm d}M}{{\rm d}\tau_M} \right) \right]_{M(t-t')}$$

and

$$\left[R_{f(M_1)} \right]_{M_1(t-t')} = \left[f(M_1) R_i(M_1) \left(-\frac{{\rm d}M_1}{{\rm d}\tau_{M_1}} \right) \right]_{M_1(t-t')}.$$

The first term on the r.h.s. is the depletion of the ISM because of the star formation process that consumes the interstellar matter; the following three terms at the r.h.s. are the contributions of single stars to the enrichment of the element i, the fifth term is the contribution by the primary star of a binary system, the sixth term is the contribution of Type Ia SNe, the following term describes the infall of primordial material, and finally the last one takes into account the eventual outflow of matter at the onset of the galactic wind in elliptical galaxies. $f(M_1)$ is the distribution function of the primary M_1 mass in a binary system, between $M_{1,\,\rm min} = M_{\rm b,\,l}/2$ and $M_{1,\,\rm max} = M_{\rm b,\,u}$. $R_{\rm SNI}$ is the rate of Type Ia SNe rate, while $E_{{\rm SNI},\,i}$ is the ejecta of the chemical element i always in Type Ia SNe. Further details on the calculation of yields and the adopted formalism can be found in Chiosi & Maeder (1986), Matteucci & Greggio (1986), and Portinari et al. (1998). For a complete presentation of the equations of chemical evolution, see Cassarà (2012).

2.2.5 Initial mass function

In literature, there are several possible laws for the IMF: at least nine according to Cassarà (2012); Cassarà et al. (2013) have derived the SSP photometry in presence of dust for all of them. In this paper, for the sake of simplicity we consider the classical Salpeter's law

$${\rm d}N = \phi(M){\rm d}M \propto M^{-2.35}{\rm d}M, \quad (11)$$

where the proportionality constant is fixed by imposing that the fraction ζ of the IMF mass comprised between $\simeq 1\,{\rm M}_\odot$ (the minimum mass whose age is comparable to the age of the Universe) and the upper limit $M_{\rm u}$ ($\simeq 100\,{\rm M}_\odot$), i.e. the mass interval effectively contributing to nucleosynthesis. Accordingly,

$$\zeta = \int_1^{M_{\rm u}} M\phi(M){\rm d}M \Big/ \int_{M_{\rm l}}^{M_{\rm u}} M\phi(M){\rm d}M. \quad (12)$$

2.2.6 *Star formation rate*

We adopt the classical law by Schmidt (1959). The SFR, i.e. the number of stars of mass M born in the time interval dt and mass interval dM, is $\mathrm{d}N/\mathrm{d}t = \Psi(t)\Phi(M)\mathrm{d}M$. The rate of star formation $\Psi(t)$ is the Schmidt (1959) law which, adopted to our model $\Psi(t) = \nu M_{\rm g}(t)^k$ and normalized to $M_{\rm B}(t_{\rm G})$, becomes

$$\Psi\,(t) = \nu M_{\rm B}\,(t_G)^{k-1}\,G\,(t)^k\,. \tag{13}$$

The parameters ν and k are crucial: k yields the dependence of the SFR on the gas content; current values are $k = 1$ or 2. The factor ν measures the efficiency of the star formation process. In this type of model, because of the competition between gas infall, gas consumption by star formation, and gas ejection by dying stars, the SFR starts very low, grows to a maximum and then declines. The time-scale τ of equation (1) roughly corresponds to the age at which the star formation activity reaches the peak value.

The chemical models for pure spheroids and/or discs provide the mass of stars, $M_*(t)$, the mass of gas $M_{\rm g}(t)$ and the metallicity $Z(t)$ that are used as entries for the population synthesis code. In the case of composite galaxies made of a disc and a bulge, the mass of the galaxy is the sum of the two components. The assumption is that disc and bulge evolve independently and each component will have its $M_*(t)$, $M_{\rm g}(t)$ and $Z(t)$.

2.3 Stars and ISM: their spatial distribution

In most EPS models, in particular those that neglect the presence of an ISM in form of gas and dust, the SED of a galaxy is simply obtained by convolving the SSP spectra with the star formation history (SFH; Arimoto & Yoshii 1987; Bressan et al. 1994; Tantalo et al. 1998) and no effect of the spatial distribution of the various components (stars and ISM) is considered. For intermediate-type galaxies with a disc and a bulge (and maybe even a halo), the situation is mimicked by considering different SFHs for the various components (Buzzoni 2002, 2005; Piovan et al. 2006b). This simple approach can no longer be used in presence of the ISM and of the absorption and IR/sub-mm emission of radiation by dust. In particular, the emission requires a spatial description, whereas the sole treatment of the extinction could be simulated by applying a suitable extinction curve. In the general case of dust extinction/emission (Silva et al. 1998; Piovan et al. 2006b), the spatial distribution of the ISM, dust, and stars in the galaxy must be specified. The observational evidence is that the spatial distribution of stars and ISM depends on the galaxy morphological type and that it can be reduced to: pure spheroids, pure discs, and composite systems made of spheroid plus disc in different proportions (here the irregulars are neglected). Therefore, one needs a different geometrical description for the various components, to each of which a suitable star formation history is associated. Finally, in the present approach, no bursts of star formation are included into the chemical model (see Piovan et al. 2006b, for some examples of starburst model galaxies). In the following, we adopt the same formalism proposed by Piovan et al. (2006b) which is also reported here for the sake of completeness and easy understanding by the reader. The formalism is presented in order of increasing complexity.

2.3.1 *Disc galaxies*

The mass density distribution of stars (ρ_*), diffuse ISM ($\rho_{\rm ISM}$), and MCs ($\rho_{\rm MC}$), inside a galactic disc is approximated to a double decreasing exponential law. Considering a system of polar coordinates with origin at the galactic centre $[r, \theta, \phi]$, the height above the equatorial plane is $z = r\cos\theta$ and the distance from the galactic centre along the equatorial plane is $R = r\sin\phi$; ϕ is the angle between the polar vector r and the z-axis perpendicular to the galactic plane passing through the centre. The azimuthal symmetry rules out the angle ϕ. The density laws for the three components are

$$\rho^i = \rho_0^i \exp\left(\frac{-r\sin\theta}{R_{\rm d}^i}\right) \exp\left(\frac{-r|\cos\theta|}{z_{\rm d}^i}\right), \tag{14}$$

where 'i' can be '$*$', 'ISM', 'MCs', i.e. stars, diffuse ISM, and star-forming MCs. $R_{\rm d}^*$, $R_{\rm d}^{\rm MC}$, $R_{\rm d}^{\rm ISM}$ are the radial scalelengths of stars, MCs, and ISM, and $z_{\rm d}^*$, $z_{\rm d}^{\rm MC}$, $z_{\rm d}^{\rm ISM}$ the corresponding scale-heights above the equatorial plane. As a first approximation, stars and star-forming MCs have the same distribution: $R_{\rm d}^* = R_{\rm d}^{\rm MC}$, and $z_{\rm d}^* = z_{\rm d}^{\rm MC}$. The scale parameters are chosen taking into account the observations for the type of object to model: for the disc of a typical massive galaxy like the Milky Way (MW), the typical assumption is $z_{\rm d} \simeq 0.3$–0.4 kpc, and $R_{\rm d}$ is derived from either observations of the gas and star distribution or from empirical relations [Im et al. (1995), $\log(R_{\rm d}/{\rm kpc}) \sim -0.2M_{\rm B} - 3.45$, where $M_{\rm B}$ is the absolute blue magnitude]. Typical values for $R_{\rm d}$ are around 5 kpc.

The constants ρ_0^i vary with the time step. Indicating with $t_{\rm G}$ the age of the model galaxy, the gaseous components need the normalization constants $\rho_0^{\rm MC}(t_G)$ and $\rho_0^{\rm ISM}(t_{\rm G})$ since both lose memory of their past history. For the stellar component, $\rho_0^*(t)$ is needed all over the galaxy life $0 < t < t_{\rm G}$. The stellar emission is calculated using the mix of stellar populations of any age $\tau' = t_{\rm G} - t$. The normalization constants come by integrating the density laws over the volume and by imposing the integrals to equal the mass obtained from the chemical model. The mass of each component $M_i(t)$ is

$$M^i = \int_V \rho_0^i \exp\left(-\frac{r\sin\theta}{R_{\rm d}^i}\right) \exp\left(-\frac{r|\cos\theta|}{z_{\rm d}^i}\right) \mathrm{d}V. \tag{15}$$

The mass of stars born at the time t is given by $\Psi(t)$: $\rho_0^*(t)$ will be obtained by using $M_*(t) = \Psi(t)$. $M^{\rm ISM}(t)$ is the result of gas accretion, star formation, and gas outflows by dying stars. The current total mass $M^{\rm MC}(t_{\rm G})$ is a fraction of $M^{\rm ISM}(t)$ and the remaining is the gas component $M_{\rm g}(t)$. The double integral (in r and θ) is numerically solved for $\rho_0^i(t)$ to be used in equation (14). The galaxy radius $R_{\rm gal}$ is left as a free parameter of the model.

The last point is the sub-division of the whole volume of a disc galaxy into a number of sub-volumes. The energy source inside each of these can be approximated to a point source located in their centres, and the coordinates $[r, \theta, \phi]$ are divided in suitable intervals. As far as the radial coordinate, $n_{\rm r} = 40$–60 is a good approximation in securing the overall energy balance among the sub-volumes, speeding up the computational time and yielding numerically accurate results. The number of radial intervals come by imposing that the mass density among two adjacent sub-volumes scales by a fixed ratio $\rho_j/\rho_{j+1} = \zeta$, with constant ζ. The grid for the angular coordinate θ is chosen in such a way that spacing gets thinner approaching the equatorial plane. We split the angle θ going from 0 to π in n_θ sub-values. We need an odd value for n_θ so that we have $(n_\theta - 1)/2$ sub-angles per quadrant. The angular distance α_1 between the two adjacent values of the angular grid is chosen following Silva (1999): $R_{\rm gal}$ subtends a fraction $f < 1$ of the disc scaleheight ($z_{\rm d}$). The grid for the angular coordinate ϕ is chosen to be suitably finely spaced near $\phi = 0$ and to get progressively broader and broader moving away clockwise and counterclockwise from $\phi = 0$.

2.3.2 *ETGs and bulges*

The luminosity distribution of ETGs is customarily described by the King law. Following Fioc & Rocca-Volmerange (1997), we use a density profile slightly different from the King law to secure a smooth behaviour at the galaxy radius $R_{\rm gal}$. The mass density profiles for stars, MCs, and diffuse ISM are

$$\rho^i = \rho_0^i \left[1 + \left(\frac{r}{r_{\rm c}^i}\right)^2\right]^{-\gamma_i}, \quad (16)$$

where as usual 'i' stands for '$*$', 'ISM', 'MCs'. $r_{\rm c}^*$, $r_{\rm c}^{\rm MC}$, $r_{\rm c}^{\rm M}$ are the core radii of the distributions of stars, MCs, and diffuse ISM; the exponents γ_* and $\gamma_{\rm MC}$ can be 1.5 (Piovan et al. 2006b) and $\gamma_{\rm ISM}$ is not well known. Froehlich (1982), Witt, Thronson & Capuano (1992), Wise & Silva (1996) suggest to adopt $\gamma_{\rm M} \simeq 0.5$–$0.75$ for the elliptical galaxies. Here, we consider $\gamma_{\rm M} = 0.75$. The density profile has to be truncated at the galactic radius $R_{\rm gal}$, free parameter of the model, to prevent the mass $M(r) \rightarrow \infty$ for $r \rightarrow \infty$. The constants $\rho_0^i(t)$, $\rho_0^{\rm MC}(t_G)$, $\rho_0^{ISM}(t_{\rm G})$ can be found by integrating the density law over the volume and by equating this value of the mass to the correspondent one derived from the global chemical model. The last step is to fix the spacing of the coordinate grid (r, θ, ϕ). The spherical symmetry simplifies this issue. and the spacing of the radial grid is made keeping in mind the energy conservation constrain. We use a sufficiently large number of grid points $n_r \simeq$ 40–60. The coordinate ϕ is sub-divided into an equally spaced grid, with n_ϕ elements in total, and $\phi_1 = 0$. For the azimuthal coordinate θ, we adopt the same grid we have presented for the discs.

2.3.3 *Intermediate-type galaxies*

Intermediate-type galaxies go from the early S0 and Sa (big bulge) to the late Sc and Sd (small or negligible bulge). Different SFHs for the disc and the bulge can reproduce this behaviour. We adopt a system of polar coordinates with origin at the galactic centre (r, θ, ϕ): azimuthal symmetry rules out the coordinate ϕ. In the disc, the density profiles for the three components are the double decreasing exponential laws of equation (14) and the scalelengths are $R_{\rm d,B}^*$, $R_{\rm d,B}^{\rm M}$, $R_{\rm d,B}^{\rm MC}$, $z_{\rm d,B}^*$, $z_{\rm d,B}^{\rm M}$, $z_{\rm d,B}^{\rm MC}$ (suffix B indicates the *disc–bulge composite model*). In the bulge, the three components follow King-like profiles (equation 16) with the core radii $r_{\rm c,B}^*$, $r_{\rm c,B}^{\rm M}$, $r_{\rm c,B}^{\rm MC}$ referred to the bulge. The SFHs of disc and bulge evolve independently: the total content in stars, MCs, and ISM is the sum of the disc and bulge contributions.

The composite shape of the galaxy leads the definition of *a new mixed grid sharing the properties of both components*. $R_{\rm B}$ is the bulge radius, $R_{\rm gal}$ the galaxy radius. The radial grid is defined building two grids of radial coordinates, $r_{{\rm B},i}$ and $r_{{\rm D},i}$. The grid of the bulge is thicker towards the centre of the galaxy: if $r_i < R_{\rm B}$, the coordinates $r_{i,\,{\rm B}}$ of the bulge grid are considered, while for $r_i > R_{\rm B}$ the coordinates of the disc $r_{{\rm D},i}$, until $R_{\rm gal}$, are used. The angular coordinate θ follows the same pattern. The azimuthal grid is chosen in the same way both for the disc and the bulge, both having azimuthal symmetry.

2.3.4 *The elemental volume grid*

Given the geometrical shape of the galaxies, the density distributions of the three main components, and the coordinate grid (r, θ, ϕ), the galaxy is subdivided into (n_r, n_θ, n_ϕ) small volumes V. Thereinafter, the volume $V(r_{iV}, \theta_{jV}, \phi_{kV})$ will be indicated as $V(i, j, k)$. The mass of stars, MCs, and diffuse ISM in each volume are derived from the corresponding density laws, neglecting all local gradients in ISM and MCs. The approximation works since the elemental volumes are small.

3 SYNTHETIC PHOTOMETRY OF A GALAXY

As already said, the light emitted by a galaxy has two main components: the light emitted by individual stars and the light emitted–reprocessed by the ISM. Our model of the SED emitted by galaxies of different morphological type along any direction strictly follows the formalism and results developed by Piovan et al. (2006a,b). In the following, we shortly summarize the prescriptions we have adopted to describe the stellar and ISM contributions.

3.1 The diffuse ISM: extinction, attenuation, and emission

For the sake of clarity, it is worth recalling here the main differences between dust *extinction* and dust *attenuation*. With the word extinction, we refer to the combined absorption and scattering of light by dust. The light comes from a background point source while the dust is entirely foreground to the source. Its distribution is irrelevant to the total extinction since the source is a background point.

With attenuation, we refer to the net effect of dust in a complex geometrical distribution: the light sources are distributed within the dust over a certain range of depths and they can be found both in front and behind the dust (see e.g. Bruzual, Magris & Calvet 1988; Calzetti & Heckman 1999). The dust can be clumpy, smooth, or anything in between. The light sources and the dust have extended distributions and as a consequence their relative location has a major impact on the net absorbed and scattered light (now including scattering both into and out of the line of sight). Dust scattering into the line of sight produces a greyer overall attenuation than if only scattering out of the line of sight were present. The emerging SED will be bluer: this is the typical situation when studying galaxies or extended regions within galaxies.

Piovan et al. (2006a, 2011a,b,c) presented detailed studies of the extinction and emission properties of dusty ISMs. They took into account three dust components: graphite, silicates, and PAHs and reached an excellent overall agreement between theory and observational data for the extinction and emission of the ISM in the MW, Large Magellanic Cloud (LMC), and Small Magellanic Cloud (SMC). As we are now going to include their results for dusty ISMs in our model galaxies, it is wise to briefly summarize here the basic quantities and relationships in usage for the sake of completeness and clarity.

The total cross-section of scattering, absorption and extinction is given by

$$\sigma_p(\lambda) = \int_{a_{{\rm min},i}}^{a_{{\rm max},i}} \pi a^2 Q_p(a, \lambda) \frac{1}{n_{\rm H}} \frac{{\rm d}n_i(a)}{{\rm d}a} {\rm d}a, \quad (17)$$

where the index p stands for absorption (abs), scattering (sca), total extinction (ext), the index i identifies the type of grains, $a_{{\rm min},i}$ and $a_{{\rm max},i}$ are the lower and upper limits of the size distribution for the i-type of grain, $n_{\rm H}$ is the number density of H atoms, $Q_p(a, \lambda)$ are the dimensionless absorption and scattering coefficients (Draine & Lee 1984; Laor & Draine 1993; Li & Draine 2001) and, finally ${\rm d}n_i(a)/{\rm d}a$ is the distribution law of the grains (Weingartner & Draine 2001b).

Using the above cross-sections, we calculate the optical depth $\tau_p(\lambda)$ along a given path

$$\tau_p(\lambda) = \sigma_p(\lambda) \int_L n_{\rm H} {\rm d}l = \sigma_p(\lambda) \times N_{\rm H}, \quad (18)$$

where L is the optical path and all other symbols have their usual meaning. The assumption is that the cross-sections remain constant along the optical path.

$j_\lambda^{\rm small}$, $j_\lambda^{\rm big}$, and $j_\lambda^{\rm PAH}$ are the contributions to the emission by small grains, big grains, and PAHs, respectively. How these quantities are calculated is widely described in Piovan et al. (2006a) to which the reader should refer for more details. The key relationships are the following ones. The contribution to the emission by very small grains (VSGs) of graphite and silicates is

$$j_\lambda^{\rm small} = \pi \int_{a_{\rm min}}^{a_{\rm flu}} \int_{T_{\rm min}}^{T_{\rm max}} a^2 Q_{\rm abs}(a,\lambda) B_\lambda(T(a)) \times \frac{{\rm d}P(a)}{{\rm d}T} {\rm d}T \frac{1}{n_H} \frac{{\rm d}n(a)}{{\rm d}a} {\rm d}a, \quad (19)$$

where ${\rm d}P(a)/{\rm d}T$ is the temperature distribution from $T_{\rm min}$ to $T_{\rm max}$ attained by grains with generic dimension a under an incident radiation field and $B_\lambda(T(a))$ is the Planck function. $Q_{\rm abs}(a, \lambda)$ are the absorption coefficients, ${\rm d}n(a)/{\rm d}a$ is the Weingartner & Draine (2001b) distribution law for the dimensions, $a_{\rm flu}$ is the upper limit for thermally fluctuating grains, $a_{\rm min}$ is the lower limit of the distribution. The temperatures of the VSGs can fluctuate above 20 K if their energy content is small compared to the energy of the absorbed photons (Draine & Li 2001; Li & Draine 2001; Piovan et al. 2006a): the temperature distribution of VSGs has been derived following the prescriptions described in Piovan et al. (2006a). In brief, two methods are used to achieve the goal: the first one is a combination and modification of the one proposed by Guhathakurta & Draine (1989) for silicate and graphite grains and of Puget et al. (1985) for PAHs, whereas the second one stands on the exact statistical solution of the problem and it is due to Draine & Li (2001) and Li & Draine (2001). The emission by big grains of graphite and silicates is evaluated assuming that they behave like blackbodies in equilibrium with the radiation field

$$j_\lambda^{\rm big} = \pi \int_{a_{\rm flu}}^{a_{\rm max}} a^2 Q_{\rm abs}(a,\lambda) B_\lambda(T(a)) \frac{1}{n_H} \frac{{\rm d}n(a)}{{\rm d}a} {\rm d}a, \quad (20)$$

where $a_{\rm max}$ is the upper limit of the distribution and the meaning of the other symbols is the same as in equation (19).

The emission by PAHs is given by

$$j_\lambda^{\rm PAH} = \frac{\pi}{n_{\rm H} hc} \int_{\lambda_{\rm min}}^{\lambda_{\rm max}} I\left(\lambda'\right) \lambda' \int_{a_{\rm PAH}^{\rm low}}^{a_{\rm PAH}^{\rm high}} \frac{{\rm d}n(a)}{{\rm d}a} \times a^2 \left[Q_{\rm abs}^{\rm IPAH}\left(a,\lambda'\right) S_{\rm ION}\left(\lambda',\lambda,a\right) \chi_i + Q_{\rm abs}^{\rm NPAH}\left(a,\lambda'\right) S_{\rm NEU}\left(\lambda',\lambda,a\right) (1-\chi_i) \right] {\rm d}a {\rm d}\lambda', \quad (21)$$

where the ionization of PAHs is taken into account (Weingartner & Draine 2001a) and $\chi_i = \chi_i(a)$ is the fraction of ionized PAHs with dimension a. $S_{\rm ION}\left(\lambda',\lambda,a\right)$ and $S_{\rm NEU}\left(\lambda',\lambda,a\right)$ give the energy emitted at wavelength λ by a molecule of dimension a, as a consequence of absorbing a single photon with energy hc/λ'. $a_{\rm PAH}^{\rm low}$ and $a_{\rm PAH}^{\rm high}$ are the limits of the distribution and $I\left(\lambda'\right)$ is the incident radiation field.

3.2 Dust-free and dust-embedded SSPs

In the following, we group the SSPs according to whether or not they incorporate the effect of dust during the MC phase of the young massive stars. In all cases, the effect of the self-absorbing envelopes of the AGB phase of intermediate- and low-mass stars is taken into account.

(i) *Dust-free SSPs.* These SSPs describe the situation in which a generation of stars has already evaporated the parental MC in which it was embedded. This implies that a certain amount of time has already elapsed from the initial star-forming event. These SSPs no longer need to include the effects of self-obscuration and radiation reprocessing exerted by the parental MC or local ISM. However, they still include these effects when caused by the dust shells surrounding the AGB stars. For these SSPs, we consider the recent study by Cassarà et al. (2013) in which the new models of TP-AGB stars by Weiss & Ferguson (2009) have been used. The reader should refer to Cassarà et al. (2013) for all details.

(ii) *SSPs-embedded in dusty MCs.* In the early stages of their evolution, we can consider stars as still heavily obscured by their parental dusty MCs. Libraries of these SSPs have been presented in Piovan et al. (2006a) as a function of four parameters: (1) optical depth τ, (2) metallicity Z, (3) PAHs ionization state (three possibilities, that is, PAHs ionized with full calculations of the ionization state, neutral PAHs, and ionization state of the PAHs as in a mixture of cold neutral matter, warm neutral matter, and warm ionized matter in the same relative proportions as in the MW), and, finally, (4) the abundance of carbon in VSGs. These libraries are still up-to-date because no significant changes have been made to the structure and evolution of massive stars in the meantime. Therefore, for these SSPs we adopt, the library by Piovan et al. (2006a), in which the absorption and emission of the radiation emitted by the young stars embedded in MCs are accurately calculated. The high density in the regions of star formations requires the solution of the radiative transfer equation, and to this purpose we adopt the robust and simple 'ray-tracing' technique. The method solves the radiative transfer equation along a set of rays traced throughout the inhomogeneous spherical symmetric source, and the spherical symmetry of the problem allows us to calculate the specific intensity of the radiation field at any point at a certain distance from the centre of the MC by averaging the intensities of all rays passing through that point. More details are given in Takagi, Vansevicius & Arimoto (2003). The Piovan et al. (2006a) SSPs, however, neglect the effects by self-contamination in AGB stars. Although complete sets of SEDs with all these effects simultaneously taken into account would be desirable, or in other words the Piovan et al. (2006a) SSPs should be folded into those of Cassarà et al. (2013), the above approximation is fully acceptable for a number of reasons: (1) the spectral regions interested by AGB stars do not coincide with the spectral regions interested by the interaction of young stars with the dust of the MCs; (2) the details of the SEDs caused by the transfer of energy from far-infrared (FIR) to near- infrared (NIR) are found to play a marginal role; (3) even if self-absorption by the AGB dusty envelopes is included, the effect is found to be marginal unless very high optical depths are chosen for the cloud.

In the following, we adopt the SSPs by Piovan et al. (2006a) up to the evaporation of the parental MC and switch to those by Cassarà et al. (2013) afterwards.

3.3 MCs and their evaporation

According to the current view of star formation, stars are born and live for part of their life inside MCs. As already recalled, the radiation emitted by these stars in the UV region of the spectrum is absorbed by MCs and re-emitted in the infrared. Therefore, the radiation emitted by a galaxy can be severely altered by the presence of the MCs. The ideal approach would be to be able to follow the evolution of MCs that are gradually consumed by the star-forming process and swept away by the radiation emitted by the underneath stars (SNe explosions and stellar winds of massive stars). A task that goes beyond the aims of this study and that is simplified by evaluating the time-scale for the MC evaporation. In the real case, however, the clouds are destroyed on a time-scale of the order of 10 Myr on average. With a good approximation, this value seems to reproduce the typical lifetime of the MCs, as discussed by Dwek (1998) and Zhukovska, Gail & Trieloff (2008). A simple way to simulate the process above is to assume that as the time goes on, the SSPs fluxes reprocessed by dust decrease, while the amount of flux left unprocessed increases. The time-scale, t_0, for the evaporation of the MC will depend on the properties of the ISM, the efficiency of the star formation and the energy injection by young stars inside. We expect t_0 to be of the same order of the lifetime of massive stars (the age range going from 3 to 50 Myr). In a low-density environment with a moderate rate of star formation, t_0 is likely close to the lowest value (lifetime of the most massive stars of the population, case of a typical spiral galaxy), while t_0 will be close to the upper value in a high-density environment, (starburst galaxies) where very obscured star formation can occur in a high-density ISM, more difficult to destroy.

Finally, there is an important effect due to metallicity. See Piovan et al. (2006a) for more details.

3.4 The SED of a galaxy

The total SED emerging from the galaxy is simulated once the main physical components, their spatial distribution, the coordinate system, and the grid of elemental volumes are known, and the interaction among stars, dusty ISM, and MCs is modelled. A generic volume $V' = V(i', j', k')$ of the galaxy will receive the radiation coming from all other elemental volumes $V = V(i, j, k)$ and the radiation travelling from one volume to another interacts with the ISM comprised between them. The energy is both absorbed and emitted by the ISM under the interaction with the radiation field. Two simplifying hypotheses are followed:

(i) The dust of a generic volume V does not contribute to the radiation field impinging on the volume V'. This is due to the low optical depths of the diffuse ISM in the MIR/FIR: dust cannot effectively absorb the radiation it emits in significant amount, except for high-density regions (Piovan et al. 2006a). The incoming radiation depends only on stars and MCs.

(ii) The radiative transfer from a generic volume V to V' is calculated by means of the effective optical depth:

$$\tau_{\rm eff} = \sqrt{\tau_{\rm abs}(\tau_{\rm abs} + \tau_{\rm sca})}. \tag{22}$$

For all details, see Piovan et al. (2006a) and Silva et al. (1998).

The total radiation field incident on V' is

$$J(\lambda, V') = \sum_{i=1}^{n_r}\sum_{j=1}^{n_\theta}\sum_{k=1}^{n_\phi} \frac{V[j^{\rm MC}(\lambda, V) + j^*(\lambda, V)]}{r^2(V, V')} \times {\rm e}^{[-\tau_{\rm eff}(\lambda, V, V')]}, \tag{23}$$

where the summations are carried over the whole ranges of i, j, k with $i \neq i'$ $j \neq j'$ $k \neq k'$; $r^2(V, V')$ is the value averaged over the volume of the square of the distance between the volumes V and V'. The effective optical depth $\tau_{\rm eff}$ of equation (23) is given by

$$\tau_{\rm eff}(\lambda, V, V') = \sqrt{\sigma_{\rm abs}(\lambda)[\sigma_{\rm abs}(\lambda) + \sigma_{\rm sca}(\lambda)]} \times \int_{V(i,j,k)}^{V(i',j'k')} n_{\rm H}(l){\rm d}l. \tag{24}$$

The integral represents the number of H atoms contained in the cylinder between V and V'. The two terms $j^{\rm MC}(\lambda, V)$ and $j^*(\lambda, V)$ are the emission by MCs and stars per unit volume of $V(i, j, k)$ and they are calculated at the centre of the volume element.

To calculate $j^{\rm MC}(\lambda, V)$ and $j^*(\lambda, V)$, the fraction $f_{\rm d}$ of the SSP luminosity that is reprocessed by dust and the time-scale t_0 for this to occur are requested. The fraction is

$$f_{\rm d} = \begin{cases} 1 & t \leq t_0 \\ 2 - t/t_0 & t_0 < t \leq 2t_0. \\ 0 & t \geq 2t_0 \end{cases} \tag{25}$$

The fraction of SSP luminosity that escapes without interacting with dust is $f_{\rm f} = 1 - f_{\rm d}$. See Piovan et al. (2006a) for a detailed description of the calculations of the monochromatic luminosity of a dust-free and dust-enshrouded SSP: for sake of clarity here, we just report the emission of stars and MCs per unit volume, $j*(\lambda, V)$ and $j^{\rm MC}(\lambda, V)$:

$$j^*(\lambda, V) = \int_{2t_0}^{t_{\rm G}} \rho_*(t) L^{\rm f}_\lambda(\tau', Z){\rm d}t + \int_{t_0}^{2t_0} \left(\frac{t}{t_0} - 1\right) \rho_*(t) L^{\rm f}_\lambda(\tau', Z){\rm d}t \tag{26}$$

and

$$j^{\rm MC}(\lambda, V) = \int_{0}^{t_0} \rho_*(t) L^{\rm d}_\lambda(\tau', Z){\rm d}t + \int_{t_0}^{2t_0} \left(2 - \frac{t}{t_0}\right) \rho_*(t) L^{\rm d}_\lambda(\tau', Z){\rm d}t. \tag{27}$$

Once the incident radiation field $J(\lambda, V')$ is known, we can obtain the emission per unit volume from the dusty ISM. The azimuthal and spherical symmetries of the galaxy models become very important, and allow us to calculate the dust emission at $\phi = 0$ for all the possible values of r and θ of this 'galaxy slice'. The total radiation field per unit volume emitted by a single element is

$$j^{\rm TOT}(\lambda, V) = j^{\rm MC}(\lambda, V) + j^*(\lambda, V) + j^{\rm ISM}(\lambda, V), \tag{28}$$

where $j^{\rm ISM}(\lambda, V)$ is the radiation outgoing from a unit volume of the dusty diffuse ISM. The total outgoing emission from the volume V, $j^{\rm TOT}(\lambda, V) \times V$, is of course different from volume to volume.

The monochromatic luminosity measured by an external observer is calculated considering that the radiation emitted by each elemental volume (n_r, n_θ, n_ϕ) has to travel across a certain volume of the galaxy itself before reaching the edge, escaping from the galaxy, and being detected.

The radiation is absorbed and diffused by the ISM along this path, and the external observer will see the galaxy along a direction fixed by the angle Θ ($\Theta = 0$: galaxy seen *face-on*, $\Theta = \pi/2$ galaxy seen *edge-on*). Hence,

$$L(\lambda, \Theta) = 4\pi \sum_{i=1}^{n_r}\sum_{j=1}^{n_\theta}\sum_{k=1}^{n_\phi} V j^{\rm TOT}(\lambda, V) {\rm e}^{[-\tau_{\rm eff}(\lambda, V, \Theta)]}, \tag{29}$$

and $\tau_{\rm eff}(\lambda, V, \Theta)$ is the effective optical depth between $V(i, j, k)$ and the galactic edge along the direction. The detailed description can be found in Piovan et al. (2006b).

4 THE COMPOSITION OF DUST

To introduce this topic, it is worth a quick summary about the dust properties and mixture adopted in the models: for a much more extended analysis of this issue and all the details about the calculations of the emission/extinction effects, see Piovan et al. (2006a).

The physical properties of the interstellar grains are derived from the dust extinction curves in the UV/optical region of the spectra and the emission spectra in the infrared bands (from the NIR up to the FIR), in different physical environments. From the amount of information that can be obtained looking at the effects of extinction and emission related to dust grains, it is possible to derive the features useful to constrain and define a quasi-standard model of interstellar dust, made up of three components.

The characteristic broad bump of the extinction curve in the UV at 2175 Å and the absorption features at 9.7 and 18 μm (Draine 2003) require a two-components model, made of graphite and silicates while a population of VSGs is necessary to reproduce the emission observed by *IRAS* at 12 and 25 μm.

VSGs are not exclusively made of silicates [the 10-μm emission feature of silicates is not detected in diffuse clouds (Mattila et al. 1996; Onaka et al. 1996): more likely, they are composed by carbonaceous material with broad ranges of shapes, dimensions, and chemical structures (Desert, Boulanger & Shore (1986) and Li & Mayo Greenberg (2002) present a detailed discussion of this topic)].

The last contributors to dust are the PAH molecules, that originated the emission lines at 3.3, 6.2, 7.7, 8.6, and 11.3 μm which have been first observed in luminous reflection nebulae, planetary H II regions, and nebulae (Sellgren, Werner & Dinerstein 1983; Mathis 1990) and in the diffuse ISM with *IRTS* (Onaka et al. 1996; Tanaka et al. 1996) and *ISO* (Mattila et al. 1996). These spectral features are referred to as the aromatic IR bands.

It appears clear that any realistic model of a dusty ISM, able to explain the UV–optical extinction and the IR emission of galaxies, need the inclusion of at least three components: graphite, silicates, and PAHs. Furthermore, the big grains can be treated as in thermal equilibrium with the radiation field, while the VSGs could have temperatures above the mean equilibrium value. The properties of a mixture of grains are obtained once their cross-sections, their dimensions, and the kind of interaction with the local radiation field are known. For more information, see Piovan et al. (2006a). We only summarize here the models that inspired our three dust components ISM, with graphite, silicates, and PAHs. The cross-sections for graphite are from Draine & Lee (1984), for silicates are from Laor & Draine (1993), and PAHs are from Li & Draine (2001), taking the latest releases from the B. T. Draine web page. The extinction curves and the distribution of dust grains as a function of their dimensions are taken from Weingartner & Draine (2001b). The emission of graphite and silicates, both for thermally fluctuating VSGs and big grains in thermal equilibrium, is based upon the classical paper Guhathakurta & Draine (1989), while for PAHs we adapted Puget et al. (1985). Finally, the ionization state of PAHs is calculated with the physical models by Draine & Sutin (1987), Bakes & Tielens (1994), and Weingartner & Draine (2001a).

Table 1. Baryonic masses of galaxies or galaxy components (in units of 10^{11} $M_\odot$) and bolometric morphological parameter $S/T = L_{\rm Bulge}/L_{\rm Tot}$.

Galaxy type	Bulge	Disc	*S/T*
Sd-Irr		0.94	0.00
Sd	0.18	0.87	0.14
Sc	0.35	0.74	0.35
Sbc	0.45	0.66	0.45
Sb	0.55	0.57	0.56
Sab	0.65	0.47	0.65
Sa	0.73	0.46	0.69
S0	0.82	0.34	0.77
E-S0	0.85	0.27	0.82
Elliptical	1.18		1.00

5 PARAMETERS FOR CHEMICAL AND SPECTROPHOTOMETRIC MODELS

We summarize and shortly comment the main parameters of the chemical and companion spectrophotometric models justifying the choice we have made for each type of model galaxies.

5.1 Chemical parameters

(i) The galactic mass $M_{\rm BM}(t_{\rm G})$. In the infall models, it represents the asymptotic value reached by the baryonic component of a galaxy at the present time, the galaxy age $t_{\rm G}$. This asymptotic mass is used to normalize the gas and star masses of the galaxies. The procedure is straightforward and $M_{\rm BM}(t_{\rm G})$ strictly coincides with real baryonic mass of the galaxy at the present time in the case of disc galaxies, because their evolution is calculated in absence of galactic wind. Conversely, in the case of spheroidal systems (bulges and/or ETGs), the occurrence of galactic winds by gas heating due to SN explosion and stellar winds requires some cautionary remarks. Galactic winds take place when the gas thermal energy exceeds the gravitational binding energy and consequently gas is expelled and star formation is halted. No subsequent revival of star formation is possible in these models. Therefore, the real mass of the baryonic component coincides with the total mass of the stellar populations built up till the wind stage. This value is lower than $M_{\rm BM}(t_{\rm G})$. Keeping this in mind, also in this case the normalization mass is $M_{\rm BM}(t_{\rm G})$. For a detailed description of the galactic wind process and its effects on the masses of gas and stars, see Tantalo et al. (1996, 1998) and Cassarà (2012). Given these premises, galaxy models for bulges and discs of different masses have been calculated using the values of $M_{BM}(t_{\rm G})$ listed in columns (2) and (3) of Table 1. Remember that the real present-day mass of spheroidal systems is somewhat smaller than the listed value and also model dependent because of the occurrence of galactic winds that halt star formation and expel a sizeable fraction of the initial BM.

(ii) The ratios $R_{\rm BM}/R_{\rm DM}$ and $M_{\rm BM}/M_{\rm DM}$, the gravitational potential and the effect of DM, are both set equal to 0.16: these ratios are adapted from Bertin et al. (1992) and agree with the current cosmological paradigm (see Hinshaw et al. 2009, for all details).

(iii) The exponent k of the Schmidt (1959) SFR; all models are calculated using $k = 1$, according to Schmidt (1959).

(iii) The efficiency ν of the SFR. All bulge models have $\nu = 5$. Even if different values of ν at varying the galactic mass might be more appropriate to match real situations (Tantalo et al. 1996, 1998), we keep it constant at varying the mass. It is worth noticing that in some way the effect of ν is not expected to be as strong

as in Tantalo et al. (1996, 1998), because the mass range we are considering is much narrower than in those studies. The value we adopt can be considered typical of a system with mass of 10^{11} $M_\odot$. The efficiency ν for the discs is significantly lower: all disc models have $\nu = 0.50$ (Portinari et al. 1998), but adjusted to the value $\nu = 0.35$ in order to match the mean metallicity in a typical disc like the MW (Buzzoni 2005). If more complicated star formation laws are used to reproduce the star formation history in disc galaxies (Portinari & Chiosi 2000), the efficiency ν should be adjusted to match the observational value of the mean metallicity.

(iv) The IMF (slope and ζ). The slope is kept constant at the classical value of Salpeter, whereas the fraction ζ of the IMF containing stars able to enrich the ISM in chemical elements during the Hubble time is $\zeta = 0.5$. As pointed out in Tantalo et al. (1996), this is a good choice in order to get models with M/L_B ratios in agreement with the observational data and it allows also to be consistent with the supersolar metallicities suggested in Buzzoni (2005) for bulges in intermediate type galaxies. In the case of disc galaxies a lower value of ζ is adopted, i.e. $\zeta = 0.17$. The choice is suggested by the typical mean metallicities in discs, i.e. $Z \lesssim 0.006$–0.008 (Buzzoni 2005).

(v) The infall time-scale τ. Although the time-scale of mass accretion is often considered as a free parameter of the models, we assume $\tau = 0.3$ for all the models in order to reduce the number of free parameters and to mimic the results from the NBody-Tree-SPH (NB-TSPH) numerical simulations by Merlin et al. (2012) on the time-scale of collapse of baryonic matter and formation of the stellar content of an elliptical like object. The ever continuing, less intense star formation in disc galaxies suggests $\tau = 3$ (Portinari & Chiosi 1999, 2000).

(vi) Age of galaxies t_G: considering the ΛCDM model of the Universe and a redshift of galaxy formation $z = z_{form} = 20$, we get $t_G = 13.30$ Gyr. All galaxies are supposed to begin their star formation history at the same time, i.e. redshift.

5.2 Spectrophotometric parameters

Here, we summarize and discuss only the most important parameters, as usual distinguishing between the bulge component of an intermediate-type galaxy (or the elliptical galaxy) and the disc component (or the disc galaxy).

(i) *Spatial structure:* r_c^M is scale radius of the ISM in the King law (equation 14); we assume $r_c^M = 0.5$ kpc. In general, the gas is made up of MCs with active star formation *and* diffuse ISM. Consequently, we need the length-scales of MCs, diffuse ISM, and stars for which we assume the same value $r_c^M = 0.5$ Kpc. For the effects due to variations of scale radii, see Piovan et al. (2006a). The ratio r_c^*/r_c^M allows the distribution of gas and stars according to different scale radii. For the sake of simplicity, we assume here that both components have the same spatial distribution (see Chiosi & Carraro 2002; Cassarà 2008, 2012, for more details).
Radial and vertical mass distributions in discs: the parameters are $z_d^* = 0.4$ kpc, $z_d^{gas} = 0.4$ kpc, $R_d^* = 5$ kpc, $R_d^{gas} = 5$ kpc (see equation 15).
Mass distribution in bulges: In equation (16), we assume $\gamma_* = 1.5$, $\gamma_{MC} = 1.5$, and $\gamma_{gas} = 0.75$ as appropriate.

(ii) 'fgasmol': this parameter fixes the amount of molecular gas present in the galaxy at the age with of the peak of star formation, with respect to the total gas. This value is then used to proportionally scale the amount of MCs at different ages of the evolution of the galaxy. Indeed, we assume that star formation occurs in the cold MCs and therefore they should be dominant in the ISM at the peak of SFR. For elliptical galaxies or bulges fgasmol has been used *only* before the onset of the galactic wind, after which the star formation process halts. In ETGs and bulges fgasmol = 0.8. In disc galaxies, we assume fgasmol = 0.6 as suggested by Piovan et al. (2006b), who took into account estimates of the masses of H_2 and H I/H II obtained from observations of late-type galaxies in the local Universe;

(iii) Evaporation time t_0: in bulges and ETGs, we adopt $t_0 = 30 \times 10^6$ yr: MCs are embedded in a primordial environment of relatively high density. Consequently, a longer time-scale is required to dissolve these MCs compared to those in a normal environment such as the solar vicinity. In discs of most likely lower density, we adopt $t_0 = 6 \times 10^6$ yr. This value is taken from Piovan et al. (2006b). Furthermore, we assume that the evaporation time-scale of MCs in disc galaxies of the local Universe is the same during the whole evolutionary history as suggested by their nearly constant SFRs.

Before concluding this section, it is worth to underline that the value we have adopted for each parameter of the chemical model is quite robust and not subject to significant variations. The values adopted for these parameters lead to a satisfactory interpretation of the chemical data for a large variety of astrophysical environments (solar vicinity and galaxies of different morphological type) as discussed in studies we referred to. As for the spectrophotometric parameters, they appear to be less constrained, and we can expect variations of their values up to 5 per cent. However, variations of the spectrophotometric parameters of this amount would yield rather small effects on the resulting galaxy SEDs and colours.

6 SEDS OF GALAXIES OF DIFFERENT MORPHOLOGICAL TYPES

With the aid of the chemical models calculated for pure bulges and discs, we build now composite galaxy models going from pure bulges (spheroids) to pure discs passing through a number of composite systems with different combinations of the two components somehow mimicking the Hubble sequence of galaxy morphological types. The combinations of bulge and disc masses are listed in columns (2) and (3) of Table 1. These values are estimated taking into account the different values of the L_{Bulge}/L_{Tot} ratio that are needed to compare theoretical galaxy colours with the observed ones. In all models, the total mass is $\sim 1 \times 10^{11}$ $M_\odot$ that according to Buzzoni (2005) is typical of intermediate-type galaxies (made by bulge + disc).

6.1 SEDs at the age $t_{Gal} = 13.30$ Gyr

In this section, we present theoretical SEDs for galaxies of various morphological types, taking into account the contribution of the different physical components to the whole galaxy emission. The analysed age is the final age of the models, that it, $t = t_{Gal} = 13.30$ Gyr, calculated considering as the redshift of formation $z_{form} = 20$, in the current cosmological framework.

In the panels of Fig. 1, we show the SEDs of galaxies of different bulge to disc ratios and at the same age of 13.30 Gyr. The morphological classification of the models have been made looking at the theoretical $[B - V]$ and $[U - B]$ colours (see below). In more detail, the left-hand panel of Fig. 1 shows the SED of a pure elliptical galaxy of 10^{11} $M_\odot$ (black solid line). We show also the emission of both graphite and silicate grains (red dot–dashed line), the emission of PAHs (black dotted line), and the old stellar population the light of which is dimmed by the parent MCs (red solid line).

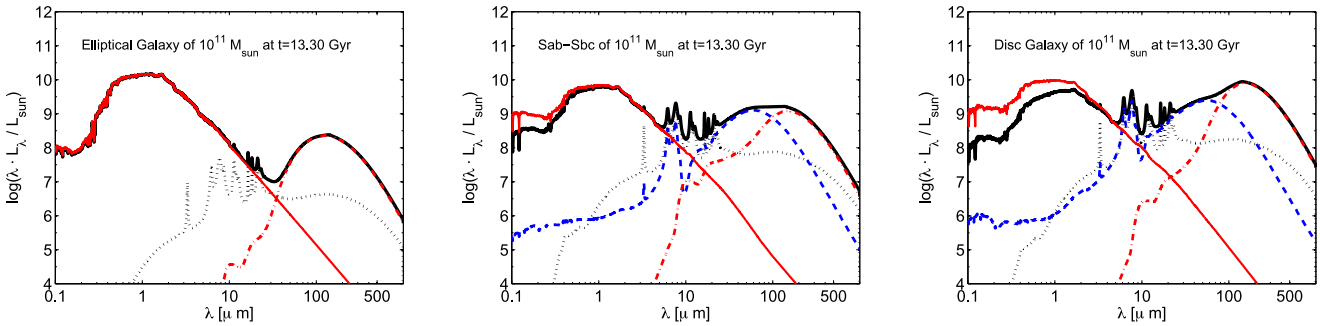

Figure 1. Left-hand panel: SED of the model elliptical galaxy of $M = 10^{11}\,\mathrm{M}_{\odot}$ (black solid line). We represent also the emission of both graphite and silicate grains (red dot–dashed line), the emission of PAHs (black dotted line), and the SED where only the extinction effect of the MCs is included (red solid line). Middle panel: the same as in the left-hand panel, but for a Sbc-Sab galaxy of $M_{\mathrm{tot}} = 10^{11}\,\mathrm{M}_{\odot}$. The meaning of the lines is the same as in left-hand panel. The blue dashed line highlights the contribution of the emission of MCs. Right-hand panel: the same as the left-hand and middle panels, but for a pure disc galaxy of $M = 10^{11}\,\mathrm{M}_{\odot}$. The meaning of the lines is always the same as before.

The middle panel displays the SED of the model Sbc-Sab galaxy, with $M_{\mathrm{Bulge}} = 0.351 \times 10^{11}\,\mathrm{M}_{\odot}$ and $M_{\mathrm{Disc}} = 0.736 \times 10^{11}\,\mathrm{M}_{\odot}$. The luminosity of the same physical components as in the left-hand panel is shown; we can observe the contribution of the emission of MCs (blue dashed line) due to the star formation still active in the disc. This effect cannot be appreciated in the case of an elliptical galaxy since the galactic wind swept off the ISM and hence stopped star formation. Together with the global EPS with the contribution of dust, we observe the emission of graphite and silicate grains, the emission of PAHs, the old stellar population extinguished *only* for the MCs effect (and not for the effect of extinction of the diffuse interstellar dust) and, finally, the emission of MCs. Finally, the right-hand panel gives the SED of a pure disc galaxy of $10^{11}\,\mathrm{M}_{\odot}$ with the contribution by the different physical components to the whole galaxy emission.

It is evident that the shape of the SEDs of the various components gradually changes passing from the elliptical model to the disc model: few differences can be observed comparing the two intermediate galaxy types.

These considerations hold for the models at 13.30 Gyr ($z = 0$).

(i) For the elliptical model, the global emission (black solid line) shows a peak in the UV (thus reproducing the UV excess observed in elliptical galaxies) and a weak IR peak, which is clearly due to a poor amount of dust grains in the diffuse medium (there is no contribution of the MCs to the emission in the IR region since star formation has stopped). As clearly explained in Bressan et al. (1994) and Yi & Yoon (2004), old, metal-rich galaxies (e.g. giant ellipticals containing even a small percentage of high-metallicity stars) naturally develop the UV upturn within a time-scale shorter than the Hubble time. No young stars are required. The stars most likely contributing to the UV flux are low-mass stars of high metallicity that, thanks to heavy mass-loss by stellar winds, evolve as hot HB burners and miss the AGB phase (see Bressan et al. 1994, for all details). Metal-poor populations produce a higher ratio of UV-to-V flux, owing to opacity effects, but only metal-rich stars develop the UV upturn, in which the flux increases towards shorter UV wavelengths. The effect of extinction is negligible as small amounts of gas and dust are expected to be present in old elliptical galaxies.

(ii) For the disc model, both the environments with the presence of dust, namely the diffuse ISM and the star-forming regions, contribute to the IR luminosity in a significant amount and both play a role in the extinction of the UV/optical radiation.

(iii) For the intermediate types (disc plus bulge), the emission of the different components is quite similar to those of the disc model. However, in the UV region, the SED where the stellar population is extinguished *only* for the MCs effect (red lines – taking into account only the effect of obscuration of young stars) and the total emission (black lines) are in practice indistinguishable for $\lambda \gtrsim 0.5$ μm, while for the disc model they are clearly separate (right-hand panel of Fig. 1). This is ultimately due to the smaller amount of gas still present in the intermediate model compared to the disc only model. In the former case, the galactic wind has pushed away out all the bulge gas, whereas in the disc the galactic wind does never occur.

The contribution of the PAHs, silicates, and graphite grains increases going from the elliptical model to the disc model; as already pointed out, this effect is due to the small amount of dust and gas present in the elliptical galaxy at the final age, whereas in disc galaxies, star formation continues until the present age. As a consequence of this, at any age, spectrophotometric models will contain *all* the physical components, i.e. newly born stars still embedded in their parental MC, stars of various ages and metallicities free from MCs and, finally, a substantial contribution of the diffuse ISM.

6.2 Disc galaxy: the effect of inclinations

Disc galaxies can be observed at different inclinations with respect to the observer. In our models, four inclinations are considered and obviously, we expect the final SED to be different according to the viewing angle, going from face-on to edge-on galaxies. The angles under consideration are: 0^0 (face-on), $\pi/6$ with respect to the z-axis perpendicular to the equatorial plane, $\pi/3$ with respect to the z-axis, and $\pi/2$ (edge-on). Differently from what happens for the models of elliptical galaxies because of their nearly spherical symmetry, the luminosity emitted from an edge-on spiral galaxy will be heavily absorbed by the equatorial dust lane between the stars and the observer, and will present a pronounced peak in the IR region of the spectrum. The same galaxy seen face-on will show a less intense FIR emission and a more intense emission in the UV/optical region compared to the edge-on model. Fig. 2 shows the total emission of the model disc galaxy of $10^{11}\,\mathrm{M}_{\odot}$ according to different inclinations. For $\lambda \geq 150$ μm, the edge-on emission of the dust is greater than the emission at all the other inclinations. The opposite in the UV–optical region: as expected, for the edge-on galaxy, the emission is lower than for the other inclinations. It is clear that every time that we consider SEDs, colours or magnitudes of dust-rich galaxies

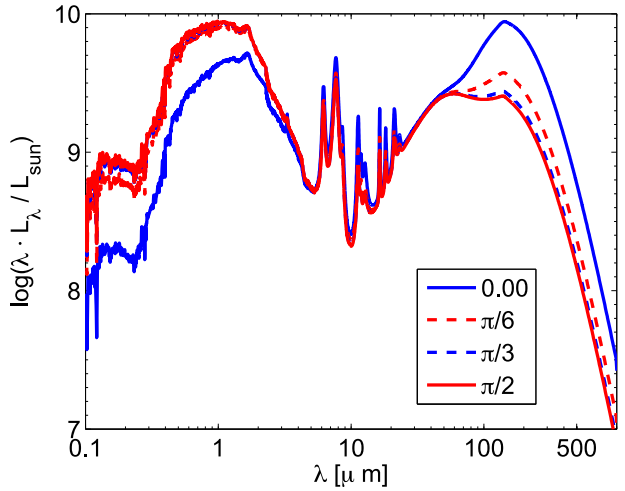

Figure 2. SED of the model disc galaxies of $M = 10^{11}$ M$_\odot$ for different viewing angles.

that are not spherically symmetric, thus introducing the dependence on the viewing angle, the results are significantly different depending on the angle. For the same model, they span a range of possible SEDs and magnitudes.

6.3 Evolutionary models of different ages

While in Section 6.1 we analysed the SEDs of galaxies at the age of 13.30 Gyr (present-day age), now we examine how the SEDs of the same models vary along their *evolutionary history*. The situation is illustrated in the various panels of Fig. 3 (upper panel: elliptical galaxy; middle panel: E-S0 galaxy; lower panel: S0 galaxy) and Fig. 4 [upper panel: Sab galaxy; lower panel: disc galaxy (Sd)] which show how the total EPS emission of the models changes at varying their age. Grouping of the models follows the morphological type, and all galaxies are supposed to start their star formation activity at redshift $z_{\rm for} = 20$. The panels show only four of the six cases reported in Table 1. They are the most representative ones of the whole sample.

Looking at the SEDs displayed in the various panels, we can make the following remarks: for the pure elliptical model at the age of $t = 0.085$ Gyr, the emission is strongly concentrated in the IR region of the spectrum: the large amount of dust present in the galaxy at this age absorbs the radiation emitted by the young stars in the UV/optical region, and it re-emits it in the IR. During this early stage, star formation occurs in media highly obscured by dust and the young stars play the dominant role in the total SED. Immediately after the onset of the galactic wind (which is supposed to occur *simultaneously and instantaneously* for the *entire* gas content of the galaxy), the gas is swept away and star formation is halted. One can assume that the star formation is virtually complete when $t = t_{\rm gw}$. We can therefore explain the SEDs of the elliptical galaxy at the ages 2.55, 5.66 and 13.09 Gyr: they represent the aging of a stellar population becoming older and older with little diffuse gas and dust content. The diffuse medium absorbs the stellar radiation in small amount, while the majority of the emission is due to cool stars in the NIR region.

For the S0 models, the presence of a small disc component allows the presence of an ever continuing star formation. It follows that, even if for $t = 0.085$ Gyr the SED is quite similar to the one of the elliptical galaxy (dust dominated emission), for older ages the

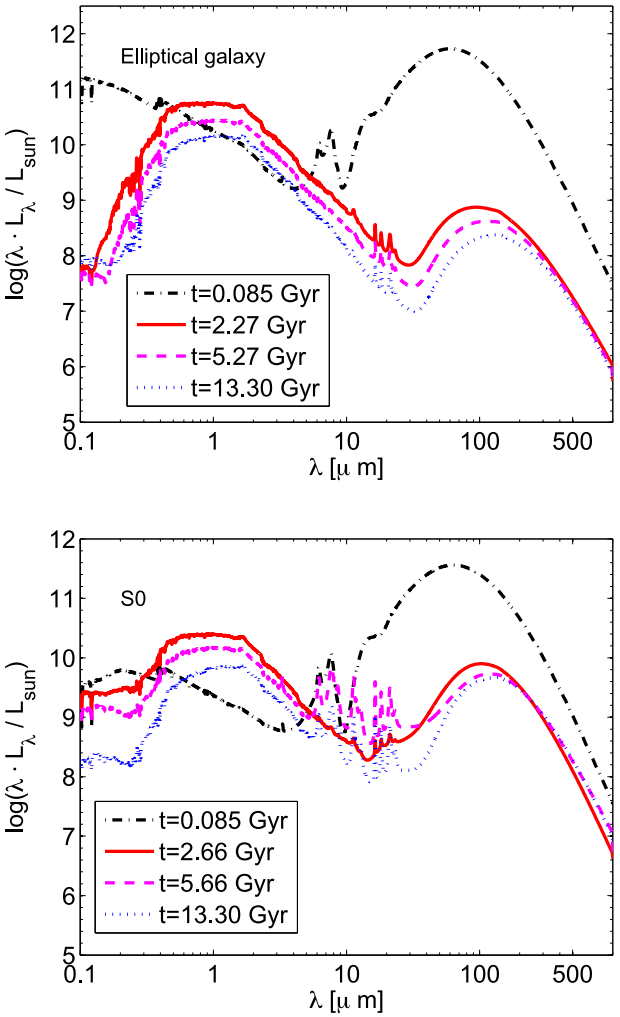

Figure 3. Time evolution of the SED of modelled galaxies of early morphological types – upper panel: elliptical; lower panel: S0 – of $M = 10^{11}$ M$_\odot$ for four significative ages, as the legend indicates.

SED is very different and the diffuse ISM significantly contributes to the MIR/FIR emission. It is also interesting to note that the PAHs features appear only after a significant enrichment in metals: this is due to the choice of the Weingartner & Draine (2001b) extinction curves. At low metallicity, we adopt their SMC flat curve with a poor or negligible contribution of the PAHs. Finally, as expected, the UV emission is much stronger than in models of elliptical galaxies; this is simply due to the small disc-like component, in which star formation never stops. The disc component could be replaced by a bulge-like component with stellar ages spanning much broader interval than in the case of a pure spheroidal galaxy.

In the Sab, Sab-Sbc, and Sd (disc) models, the disc mass, the amounts of dust, and their effects in turn grow with the morphological type. The total emission increases with time, reaches a maximum in correspondence to the peak of the star formation (both in the optical region and in the IR), and then decreases with the decrease of the SFR, according to the typical SFH adopted for discs (Piovan et al. 2006b; Cassarà 2008). As already pointed out, the SFR does not fall sharply as in the case of elliptical galaxies: it reaches a peak and then slowly declines, and continues up to the present age. It is worth noticing that for $t = 0.085$ Gyr, the SED is *clearly* split into

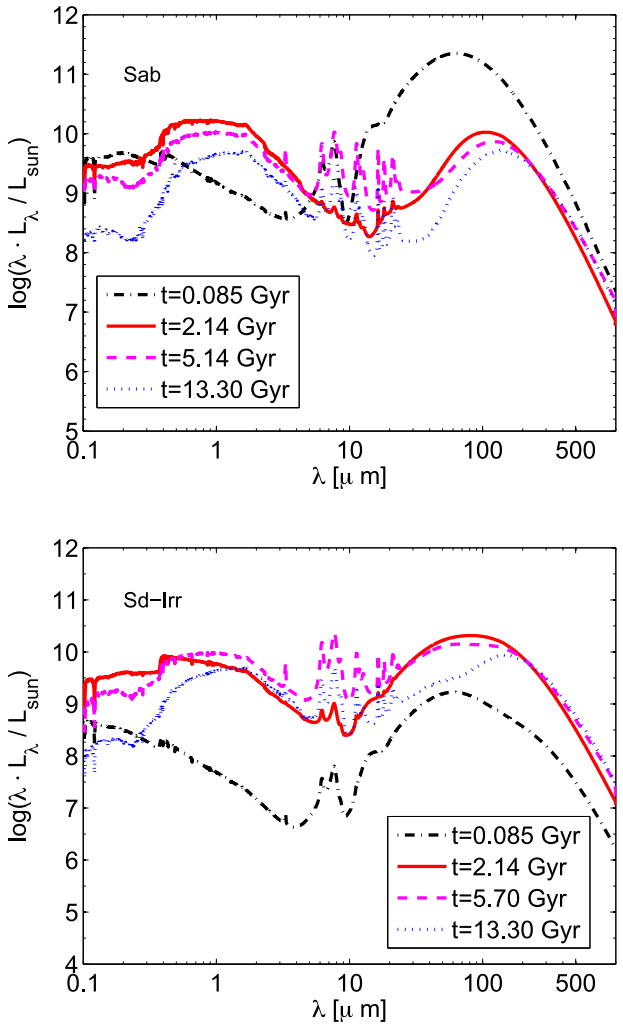

Figure 4. Time evolution of the SED of modelled galaxies of late morphological types – upper panel: Sab; lower panel: Sd-Irr (disc), of $M = 10^{11}\,\mathrm{M}_{\odot}$ for four significative ages, as the legend indicates.

two peaks (FIR and UV); as the age increases, the trend is smoothed out as intermediate-age and old stars contribute significantly to the 1 μm emission. For the late-type models, this is even more evident than for the S0 ones, the PAHs features in the SED correlate with the metallicity: the low Z extinction introduced in our models and based on the SMC extinction curve, produce young (high-z) galaxies with rather weak PAHs features.

Finally, for the full disc model, there is no phase during the early evolutionary stages where the galaxy SED is dominated by the FIR emission. As a matter of fact, we miss in this case the strong and heavily obscured burst of star formation in the bulge. Along the whole evolution, a more regular process of star formation unrolls.

7 THEORETICAL AND OBSERVATIONAL COLOURS OF GALAXIES

In this section, we examine the theoretical colours obtained from the SEDs of galaxies of different morphological types and compare them with some observational data available in the literature. Buzzoni (2005) presents a set of EPS models for template galaxies along the Hubble morphological sequence. These models account for the individual evolution of bulge, disc, and halo and provide basic morphological features, along with bolometric luminosity and colour evolution, between 1 and 15 Gyr. The integrated colours and the morphological type are tightly related: this is due to the relative contribution of stellar populations in the bulge and disc (Arimoto & Jablonka 1991).

The Buzzoni (2005) models deal with the stellar component, which is obviously the dominant contributor to the galaxy luminosity in the UV–optical region. The ISM gas has more selective effects on the SED by enhancing monochromatic emission, e.g. the Balmer lines. As far as galaxy broad-band colours are concerned, at the present age, the gas influence is negligible. Internal dust could play the dominant role, especially at short wavelength ($\lambda \lesssim 3000$ Å). Metallicity and stellar birth rate are constrained by comparing theoretical results with observational data. For all other details, see Buzzoni (2005).

Our models differ from those of Buzzoni (2005) in several aspects among which we recall: first of all, they do not consider the contribution of the halo. However, this should have a marginal effect, because the halo plays a secondary role in the mass and luminosity budget. More relevant here, our models consider the contribution of dust. In any case, we also consider the case of a dust-free ISM and hence dust-free galaxy emission (i.e. SEDs due only to stars) in order to compare the new dusty SEDs with those with no dust (Bressan et al. 1994; Buzzoni 2002, 2005). Furthermore, rather than assuming a simple prescription for the star formation law as in Buzzoni (2005), we follow the history of a galaxy with the aid of a complex model that puts together suitable prescriptions for gas infall, SFR, IMF, and stellar ejecta, all of which determine the total amounts of gas and stars present at any age together with the chemical history (Chiosi 1980; Tantalo et al. 1996, 1998; Portinari et al. 1998; Portinari & Chiosi 1999, 2000; Piovan et al. 2006b). For the SFR, we use the classical Schmidt law, whereas Buzzoni (2005) adopts the power law SFR $= Kt^{-\eta}$ with $\eta < 1$.

As already mentioned, the chemical parameters for the galaxy models are chosen in such a way that the observational values for the ratio $L_{\mathrm{Bulge}}/L_{\mathrm{Tot}}$ are reproduced (see below for more details). In contrast, for each Hubble type, Buzzoni (2005) calibrated the morphological parameter $S/T = L(\mathrm{spheroid})/L(\mathrm{tot})$. As the S/T calibration does not vary in the infrared range, he chose the I luminosity as a reference for the model setup. In our simulations, the S/T ratio cannot be determined a priori; indeed, we start from the SED of a certain model galaxy, of which we know the asymptotic infall mass *in advance*. The SED is fed to the photometric code, which calculates colours and magnitudes in different photometric systems. In our case, the disc and bulge luminosities are used a posteriori to get clues about the asymptotic mass of the galaxy that should be used as input. Carefully tuning this procedure, one may eventually obtain the correct initial values for the disc and bulge mass consistent with the S/T ratios of the different morphological types. Assuming the metallicity (and hence ζ, τ, and ν), there is an *almost-linear* relation between the bulge mass (the mass of the disc follows from $\mathrm{M}_{\mathrm{disc},\odot} = 10^{11} - \mathrm{M}_{\mathrm{bulge},\odot}$ because all the intermediate types have the same total mass of $10^{11}\,\mathrm{M}_{\odot}$) and the luminosity.

As explained in Buzzoni (2005), observations of the central bulge of the MW show that it mainly contains metal-rich stars (Frogel 1988, 1999) and this seems to be quite common also among external galaxies (Jablonka, Arimoto & Martin 1996; Goudfrooij, Gorgas & Jablonka 1999; Davidge 2001). The exact average value of the bulge metallicity has been subject to continuous revision,

going from [Fe/H] $\sim +0.2$ (Whitford & Rich 1983; Rich 1990; Geisler & Friel 1992) to lower values, consistent with a standard or even slightly sub-solar metallicity (Tiede, Frogel & Terndrup 1995; Sadler, Rich & Terndrup 1996; Zoccali et al. 2003; Origlia, Valenti & Rich 2005). According to these arguments, for the bulge of his intermediate-type galaxies, Buzzoni (2005) adopts SSPs with [Fe/H] $= +0.22$ in agreement with the observations of external galaxies. For the disc component, relying on the observed colours of present-day galaxies, Buzzoni (2005) adopts $[\mathrm{Fe/H}]_{\mathrm{disc}} = -0.5$ dex as a luminosity-weighted representative value for his models.

In order to account for the prescription of Buzzoni (2005), two different sets of galactic models are calculated; their parameters are listed and discussed in Section 5. The only difference between the sets concerns the actual stellar metallicity. Our chemical code does not reach a supersolar metallicity for the bulge (unless we force the input parameters to extreme values) in particular at the lowest galaxy masses. For realistic values of the parameters, our bulges reach solar or slightly supersolar metallicities. Also for the disc, we cannot easily reach the low value suggested by Buzzoni (2005): the metallicity of our discs tends to be slightly higher. The fundamental parameter to vary is ζ. Slightly supersolar metallicities (for the bulge) and slightly lower than the average LMC value (for the disc) are the best values that can be obtained for plausible values of ζ in the Salpeter IMF in model galaxies with total asymptotic mass of $10^{11}\,\mathrm{M}_{\odot}$. We keep these values in order to maintain the general property that in any case the bulge ($Z \gtrsim 0.02$) is more metal rich than the disc ($Z \lesssim 0.008$). In order to evaluate the effect due to different values of the metallicity for the two galaxy components, disc, and bulge, we calculate two different set of models.

(i) The first set stands on the parameters already discussed in Section 5. In this case, the galactic code, performing the EPS, will interpolate between SEDs of SSPs taking for each of them the metallicity predicted by the chemical code at the time when that stellar population was born.

(ii) The second set stands on the same parameters, but in this case we force the galactic code to generate the same metallicities adopted by Buzzoni (2005) for the disc and bulge. In this case, there is no interpolation on the SEDs of SSPs in metallicity, because it is fixed for both disc and bulge.

The results of our simulations, together with the observed colours, are shown in Figs 5–7. They show galaxy colour distributions, that is $[B-V]$ versus bolometric morphological parameter $S/T = L_{\mathrm{Bulge}}/L_{\mathrm{Tot}}$ (upper panel) and $[U-B]$ versus bolometric morphological parameter $S/T = L_{\mathrm{Bulge}}/L_{\mathrm{Tot}}$ (lower panel). Data are taken from Pence (1976, magneta circles), Gavazzi et al. (1991, blue squares), Roberts & Haynes (1994, red stars) and Buta et al. (1994, black triangles). The red star located at $\sim S/T = 1$ is the mean colour for elliptical galaxies by Buzzoni (1995). We show also the theoretical colours (filled black circles) predicted by Buzzoni (2005) for the sake of comparison. All galaxy colours have been corrected for reddening. In Fig. 5, our theoretical colours are indicated with blue diamonds and red triangles: they have been calculated using EPS with and without dust extinction, e.g. the classical bare EPS of Bressan et al. (1994), respectively. For these models, we fix only the chemical parameters (see Section 5) and let the spectrophotometric code free to interpolate in metallicity, according to the input values provided by the chemical models. In Fig. 7, our theoretical colours are indicated with black stars and red diamonds depending on whether EPS with or without dust are used. For these models, we impose that the spectrophotometric code uses the metallicities

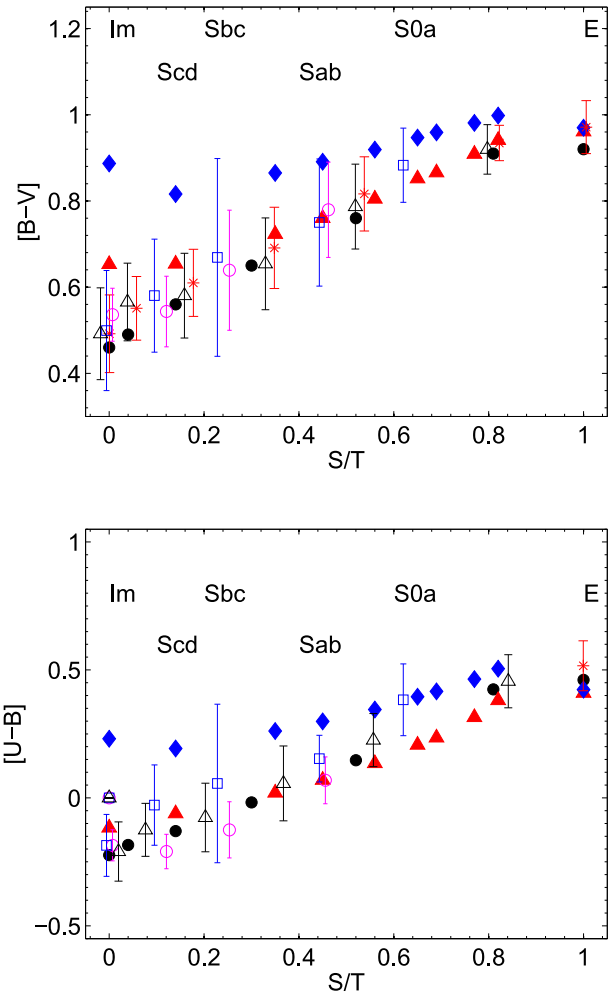

Figure 5. Galaxy colour distribution (upper panel: $[B-V]$ versus bolometric morphological parameter $\mathrm{S/T} = L_{\mathrm{Bulge}}/L_{\mathrm{Tot}}$; lower panel: $[U-B]$ versus bolometric morphological parameter $S/T = L_{\mathrm{Bulge}}/L_{\mathrm{Tot}}$). Data are from Pence (1976, magneta circles), Gavazzi, Boselli & Kennicutt (1991, blue squares), Roberts & Haynes (1994, red stars), and Buta et al. (1994, black triangles). All the data have been properly corrected by dust extinction. The red star located at $\sim S/T = 1$ represents the mean colour for EGs (Buzzoni 1995). Our theoretical colours are indicated with blue diamonds and red triangles: they have been calculated, respectively, by means of the EPS with dust and EPS corrected for the contribution of dust. For the sake of comparison, in these panels we report the theoretical colours predicted by the models of Buzzoni (1995, black circles).

of the disc and bulge indicated by Buzzoni (2005), in such case no interpolation of the SSP SEDs in metallicity is applied. Finally, in Fig. 6, only theoretical colours generated by SEDs of EPS *with dust* are plotted, but taking into account the effect of the viewing angle.

The agreement of our simulations with the data is good and the following considerations can be made.

(i) As expected, in all the figures, the theoretical colours best fitting the extinction-corrected data are the dust-free ones. The general trend is the same in both cases, however extinction and emission by dust affects the values of the colours. Between the classical dust-free EPS and those with dust, there is a difference of ~ 0.2 in both $[B-V]$ and $[U-B]$. This difference can be easily explained since the colours in the plots are all in the optical region,

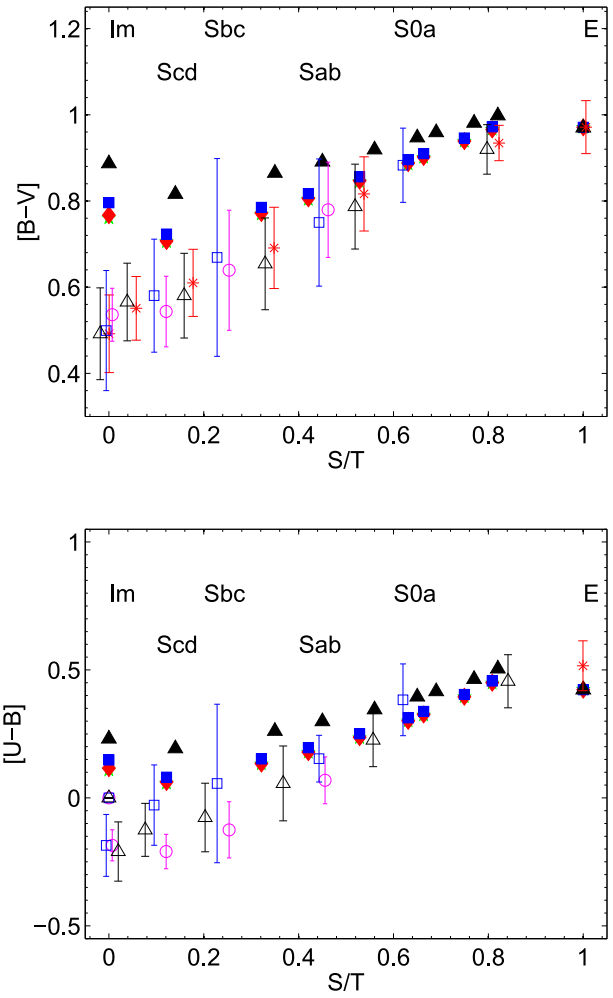

Figure 6. The same as in Fig. 5, but now only theoretical colours for EPS with dust are shown: the different symbols and colours indicate different viewing angles. Black triangles: galaxy seen edge-on; blue squares: galaxy observed at an angle of 60° measured respect to the galactic equatorial plane; red diamonds: galaxy observed at an angle of 30° measured respect to the galactic equatorial plane; green stars: galaxy seen face-on.

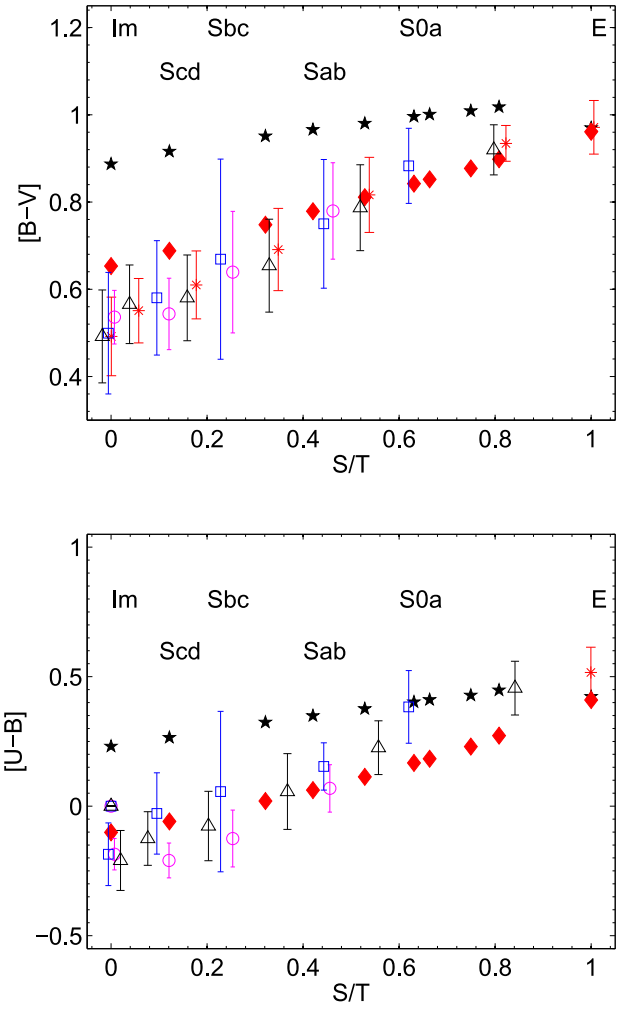

Figure 7. As in Fig. 5, but without any interpolation on the SEDs of SSPs in metallicity, because it is fixed for both disc and bulge.

thus being all absorbed by dust, with more extinction for the bands at shorter wavelengths. A stronger difference would be observed in optical–near-IR colours, since the near-IR radiation is less absorbed by dust.

(ii) The effect of dust is more evident in the late-type galaxies, richer in gas and dust. For the models of ETGs, at the present age (all the models have been calculated from $z = z_{\rm for}$ to $z = 0$, that is $t_{\rm G} = 13.30$ Gyr) only a small amount of dust is still present (see for instance the discussion in Section 6.1). Colours obtained using EPS with or without dust are in practice indistinguishable, while the differences increase going from early-type towards late-type galaxies.

(iii) The effect of metallicity is evident *but* not so remarkable: the same trend is followed by the theoretical colours, for both cases with fixed and not fixed metallicity, see Figs 5 and 7. This suggests that our models well reproduce the observations.

(iv) The effect of the inclination of the disc strictly follows the discussion of Section 6.2: the absorption due to dust is more spectacular when the galaxies are observed edge-on.

8 COSMOLOGICAL EVOLUTION OF GALAXY COLOURS

In this section, we present the photometric evolution of our model galaxies as a function of redshift in the ΛCDM Universe we have adopted and we compare the theoretical magnitudes and colours with some available observational data.

For a source observed at redshift z, the relation between photons observed at a wavelength λ_0 and emitted at wavelength $\lambda_{\rm e}$ is $\lambda_{\rm e} = \lambda_0/(1+z)$. Furthermore, if the source has an apparent magnitude m when observed in a certain photometric passband, its absolute magnitude M in the rest-frame passband satisfies the relation

$$m = M + {\rm DM} + K_{\rm corr}, \tag{30}$$

where DM is the distance modulus and $K_{\rm corr}$ is the so-called K-correction. The distance modulus is defined by

$${\rm DM} = 5\log_{10}\left(\frac{D_{\rm L}(z)}{10\,{\rm pc}}\right), \tag{31}$$

where $D_{\rm L}(z)$ is the luminosity distance and $1\,{\rm pc} = 3.086 \times 10^{18}$ cm.

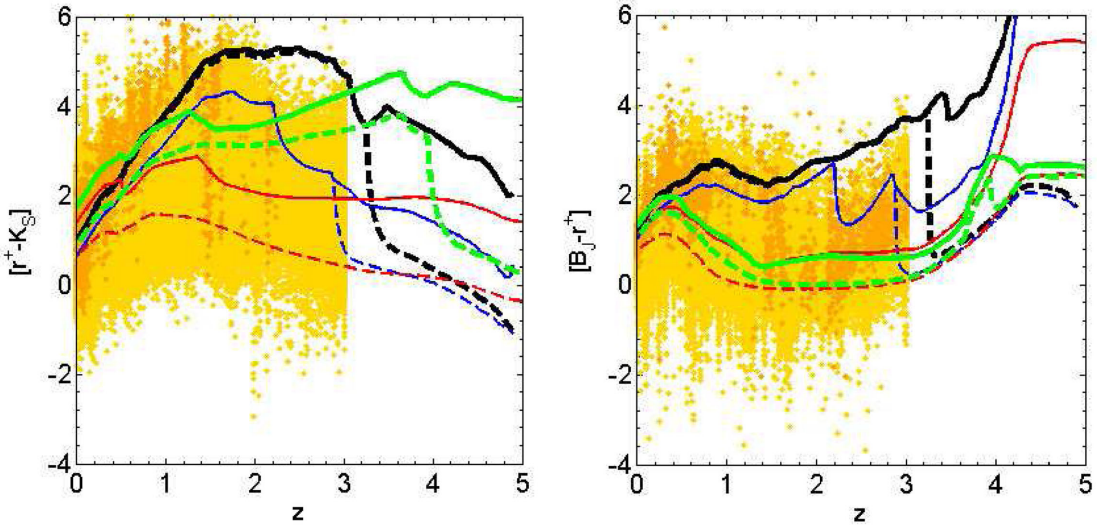

Figure 8. Left-hand panel: cosmological evolution with the redshift for the $[B_J - r^+]$ colour of the survey COSMOS (both filters are passbands of the Subaru telescope). The sample of galaxies represented is taken from the catalogue of galaxies observed in the COSMOS survey and selected in Tantalo et al. (2010). The total sample of galaxies is represented in yellow, while the ETGs are represented in orange. Superimposed, the evolution of the colour $[B_J - r^+]$ for three models presented in this work or ad hoc calculated for this redshift evolution, namely: (1) two elliptical galaxies with masses 10^{10} and 10^{12} $M_\odot$ and with the same choice of the input parameters as in Section 6.3 (black and blue lines); (2) an intermediate-type model Sab of 10^{11} $M_\odot$ (green line) and (3) a disc galaxy (Sd) of 10^{11} $M_\odot$ (red line). In all the cases, we show the evolution of the colour taking into account our dusty EPS (solid lines) and classical EPS without dust (dotted lines). Right-hand panel: The same as in the left-hand panel but for the colour $[K_S - r^+]$ of the survey COSMOS (r^+ is a filter of the Subaru telescope, while K_S is from the Kitt Peak national Observatory).

The luminosity of a source at redshift z is related to its spectral density flux (energy per unit time per unit area per unit wavelength) by

$$L(\lambda_e) = 4\pi(1+z)D_L^2 f(\lambda_0), \tag{32}$$

where $f(\lambda_0)$ is the monochromatic flux of the source at the observer. The K-correction is defined as

$$K_{\rm corr} = 2.5\ \log_{10}(1+z) + 2.5\ \log_{10}\left[\frac{L(\lambda_0)}{L(\lambda_e)}\right]. \tag{33}$$

In order to compare sources at different redshifts, we must convert the apparent photometric data (magnitudes, etc.) to rest-frame quantities by applying the K-corrections and also correct the rest-frame quantities for the expected evolutionary changes during the time interval corresponding to the redshift difference, the so-called evolutionary correction $E(z)$. The K- and E-corrections are usually derived from the theoretical SEDs calculated with the stellar EPS technique. Given the above definitions, $K(z)$ and $E(z)$ can be expressed as magnitude differences in the following way:

$$\begin{aligned} K(z) &= M(z, t_0) - M(0, t_0) \\ E(z) &= M(z, t_z) - M(z, t_0), \end{aligned} \tag{34}$$

where $M(0, t_0)$ is the absolute magnitude in a passband derived from the *rest-frame* spectrum of the source at the current time, $M(z, t_0)$ is the absolute magnitude derived from the spectrum of the source *at the current time but redshifted at* z, and $M(z, t_z)$ is the absolute magnitude obtained from the spectrum of the source *at time* t_z *and redshifted at* z. To summarize the absolute magnitude, $M(z)$, in some broad-band filter and at redshift z and its apparent magnitude $m(z)$ are expressed by

$$M(z) = -2.5 \log L(z, t(z)), \tag{35}$$

and, passing to apparent magnitudes,

$$m(z) = M(z) + E(z) + K(z) + {\rm DM}(z). \tag{36}$$

The relation between the cosmic time t and redshift z, $t(z)$, of a stellar population formed at a given initial redshift z_f, depends on the adopted cosmological model of the Universe (and its parameters).

In the next section, we will compare the SEDs of our model galaxies with the luminosities of galaxies from the Takeuchi et al. (2010) data base kindly provided us by Takeuchi (private communication). To this aim, it is useful to remind here the procedure to get the luminosities back from the apparent AB, ST, and Vega magnitudes. The luminosity in a passband satisfies the relations

$$\begin{aligned} L(\nu_0)\,\Delta\nu_0 &= L(\lambda_0)\,\Delta\lambda_0 \\ &= 10^{0.4K(z)} 4\pi D_L^2(z) \cdot \\ &\quad \times 10^{-0.4(m_{\rm AB}+48.60)} \Delta\nu_0, \end{aligned} \tag{37}$$

where $\Delta\nu_0$ and $\Delta\lambda_0$ are the integrals of the filter over the passband. Similar equations hold for the Vega and ST systems, provided that the corresponding photometric constants are used and that the monochromatic flux for the ST and Vega systems is expressed per Angstrom. The Takeuchi et al. (2010) data base yields monochromatic fluxes normalized to the pivotal wavelength that are corrected for $E(z)$ and $K(z)$, i.e. simply

$$\nu_e L(\nu_e) = 4\pi D_L^2(z)\, f(\nu_0)\, \nu_0. \tag{38}$$

8.1 Comparison with the observations

Nowadays, deep and large scale surveys, from earth and space, allow us to obtain extremely rich samples of data at different redshifts and in different wavelengths, from the UV to the FIR. The main characteristic of these deep photometric surveys detecting a

large number of galaxies is that a significant fraction of the detected objects appear as point sources. They can neither be easily distinguished from single stars, nor easily classified from a morphological point of view. It follows that the photometric study of their properties is crucial, also in order to produce some morphological classification.

In this paper, we take into account the Cosmic Evolution Survey (COSMOS) official photometric redshift catalogue (Scoville et al. 2007), designed to probe the evolution of galaxies in the context of their large-scale structure out to moderate redshift (see also Capak et al. 2007; Mobasher et al. 2007). Tantalo et al. (2010) selected an extended sample of ETGs in the COSMOS catalogue: the morphological selection is made with an automatic pipeline able to separate the objects by means of their bi-dimensional distribution of the light.

COSMOS: The panels of Fig. 8 show the evolution with redshift of the COSMOS colours $[B_J - r^+]$ (left-hand panel) and $[K_S - r^+]$ (right-hand panel) for our model galaxies of different morphological types. We show three cases: (i) a pure spheroidal system, for which two masses 10^{10} and $10^{12}\,M_\odot$ are considered (the selected sample is indeed made by ETGs); (ii) a galaxy of intermediate type Sab, characterized by a disc and a bulge, with total mass $10^{11}\,M_\odot$; (iii) finally a pure disc galaxy with no bulge (representing an Sd type). For each galaxy type, we also consider two cases, i.e. with (solid lines) and without (dashed lines) dust in the derivation of their SEDs. The colours $[B_J - r^+]$(left-hand panels) and $[K_S - r^+]$ (right-hand panels) of galaxies of the COSMOS sample are also shown. The ETGs are identified by the parameter $T_{\rm phot} \leq 1.1$ (see Tantalo et al. 2010, for more details). The yellow diamonds show the total sample of galaxies, whereas the sample of ETGs selected by Tantalo et al. (2010) is represented by the orange diamonds. For the pure spheroidal galaxy, the agreement with the data is good, at least up to redshift $z \sim 1$–1.5. In the redshift interval $0 < z < 1$, where most of the ETGs are concentrated, colours are in better agreement with the observational data. In our simulations, the galactic wind stops abruptly the process of star formation so that the galaxy evolves almost passively from the redshift of the wind $z = z_{\rm twind}$ to the present $z = 0$. We can notice that our colours extend towards the region with the yellow circles representing ETGs, in particular for the most massive galaxy $10^{12}\,M_\odot$. This interval is delicate for our models because in the chemical simulations supporting the EPS code, the galactic wind starting at $z \sim 3$ is an instantaneous process emptying the galaxy of gas; a more gradual process as we expect to happen in real galaxies would be more suitable allowing us to avoid fluctuations in the calculated colours due to the discontinuity in the evolution of the gas mass. For redshift higher than $z \sim 3$, corresponding about to the onset of the galactic wind, we have no data to test the agreement between observations and theoretical colours. We can notice the effect of dust, by comparing the dashed (without dust) and solid lines (with dust). Dust absorbs stellar radiation stronger in the B_J band than the r^+ band. Both magnitudes increase, but, since the B_J band is more absorbed, the colour becomes redder. Finally,

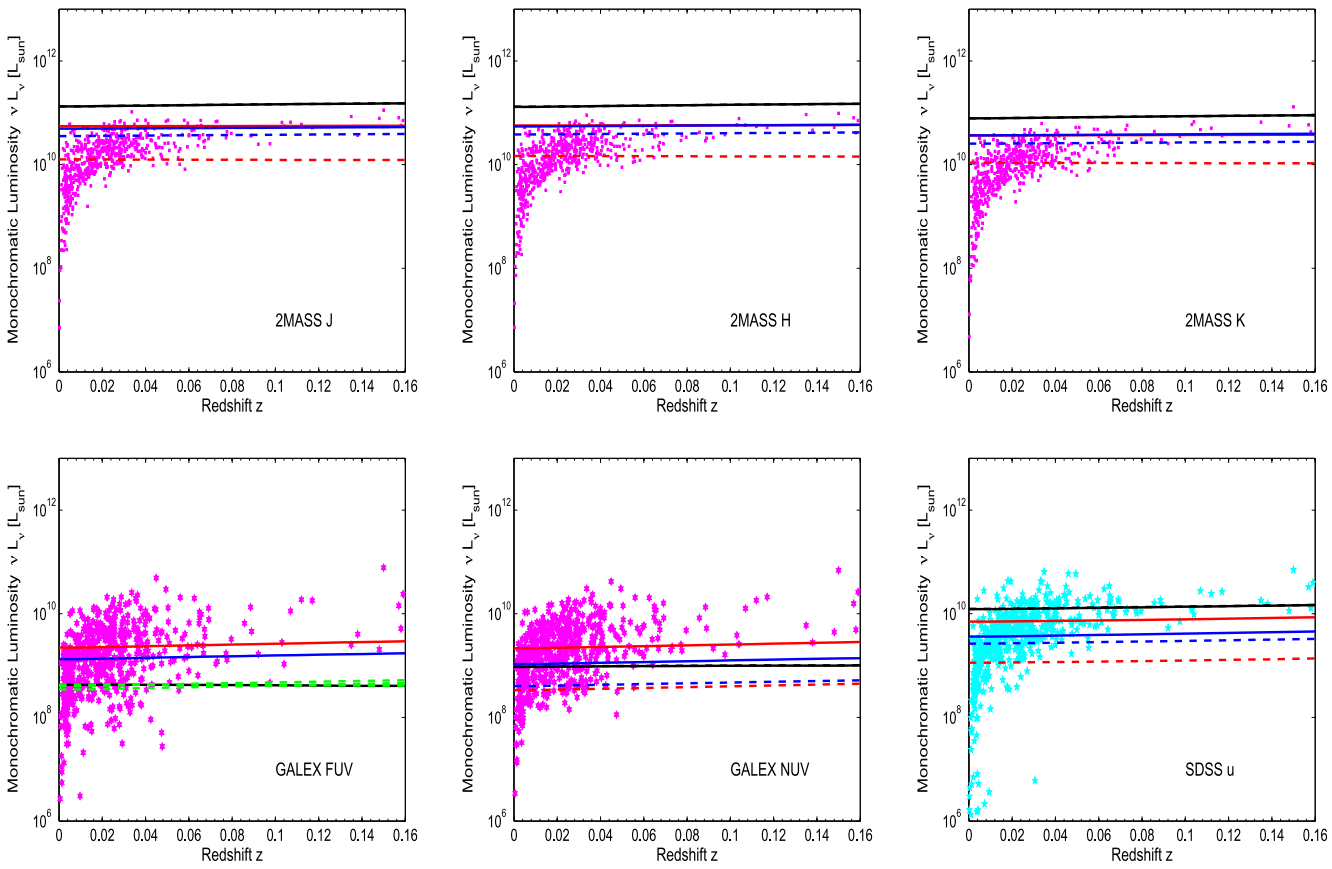

Figure 9. A comparison of the monochromatic luminosities $\nu \cdot L(\nu)$ of three models with asymptotic mass $10^{12}\,M_\odot$ with a sample of galaxies of various morphological types and masses by Takeuchi et al. (2010). We represent an elliptical galaxy (black lines), an intermediate-type galaxy (blue lines) and a disc galaxy (red lines). Solid lines represent the edge-on model, more affected by the ISM extinction, while dashed lines represent the face-on model. The pass-bands on display are *J*, *H*, and *K* bands of 2MASS, FUV, and NUV of Galex, and *u* of SDSS.

we briefly comment on the colours of galaxies of intermediate type and pure disc. The results for COSMOS are quite interesting: the colours tend to stay in the region occupied by the yellow points, exactly where there are no ETGs. In particular for the $[B_J - r^+]$, the result is good with a clearly different path in the colour–redshift plane followed by the different morphological types. In the $[K_S - r^+]$–redshift plane, again the models of disc galaxies tend to populate the region of the yellow diamonds, whereas those of the intermediate type ones fall in between the two extreme cases.

Galaxy luminosities: to conclude this section, in Figs 9 and 10 we present a simple comparison of the luminosities of our models with the data for 607 galaxies of various morphological type by Takeuchi et al. (2010) observed in different photometric systems. Of course, this sample contains objects spanning wide ranges of masses and morphological types so that much narrower grids of theoretical models would be required. This is beyond the purposes of this study and we leave it to a future work. For now, we limit ourselves to simply check that our models are consistent with the luminosity range indicated by the observations. To this aim, we plot the evolution of the monochromatic luminosity of our models for three massive galaxies (elliptical, intermediate, and disc) of about 10^{12} $M_\odot$. Since the redshift range spanned by the data (from $z = 0$ to 0.16) is rather small, we do not expect our models to evolve significantly in luminosity. This is what we see in Figs 9 and 10. The average of our models fall in the range of the observations at all pasbands, with some dispersion due to different inclinations of the disc. This effect is in particular relevant for the UV luminosities. For AKARI, since dust does not absorb its own radiation there is no difference between different inclinations and the two lines, solid and dashed one, are coincident. As expected, the model for elliptical galaxy presents a low luminosity due to the low content of dust, whereas the dust-rich morphological types better agree with the observations.

9 DISCUSSION AND CONCLUSION

In this paper, improving upon the standard EPS technique, we have developed theoretical SEDs of galaxies, whose morphology goes from disc to spherical structures, in presence of dust in the ISM. Properly accounting for the effects of dust on the SED of a galaxy increases the complexity of the problem with respect to the standard EPS theory because it is necessary to consider the distribution of the energy sources (the stars) inside the ISM absorbing and re-emitting the stellar flux. This means that the geometry and morphological type of the galaxy become important and unavoidable ingredients of the whole problem, together with the transfer of radiation from one region to another. The emergent SEDs of our model galaxies have been shown to reproduce very well, even in details, the observational data for a few test galaxies of different morphological type. The model is versatile and applicable to a large range of objects of astrophysical interest at varying the star formation and chemical enrichment histories, the geometrical shape or morphology of the galaxies, and the amounts of gas and dust contained in their ISM.

Before concluding, it is worth mentioning a few points of weakness that could be improved. First, the chemical models we have adopted are from Tantalo et al. (1996, 1998), and the chemical yields are from Portinari et al. (1998). These models are state-of-the-art in the study of the chemical evolution of galaxies. However, they

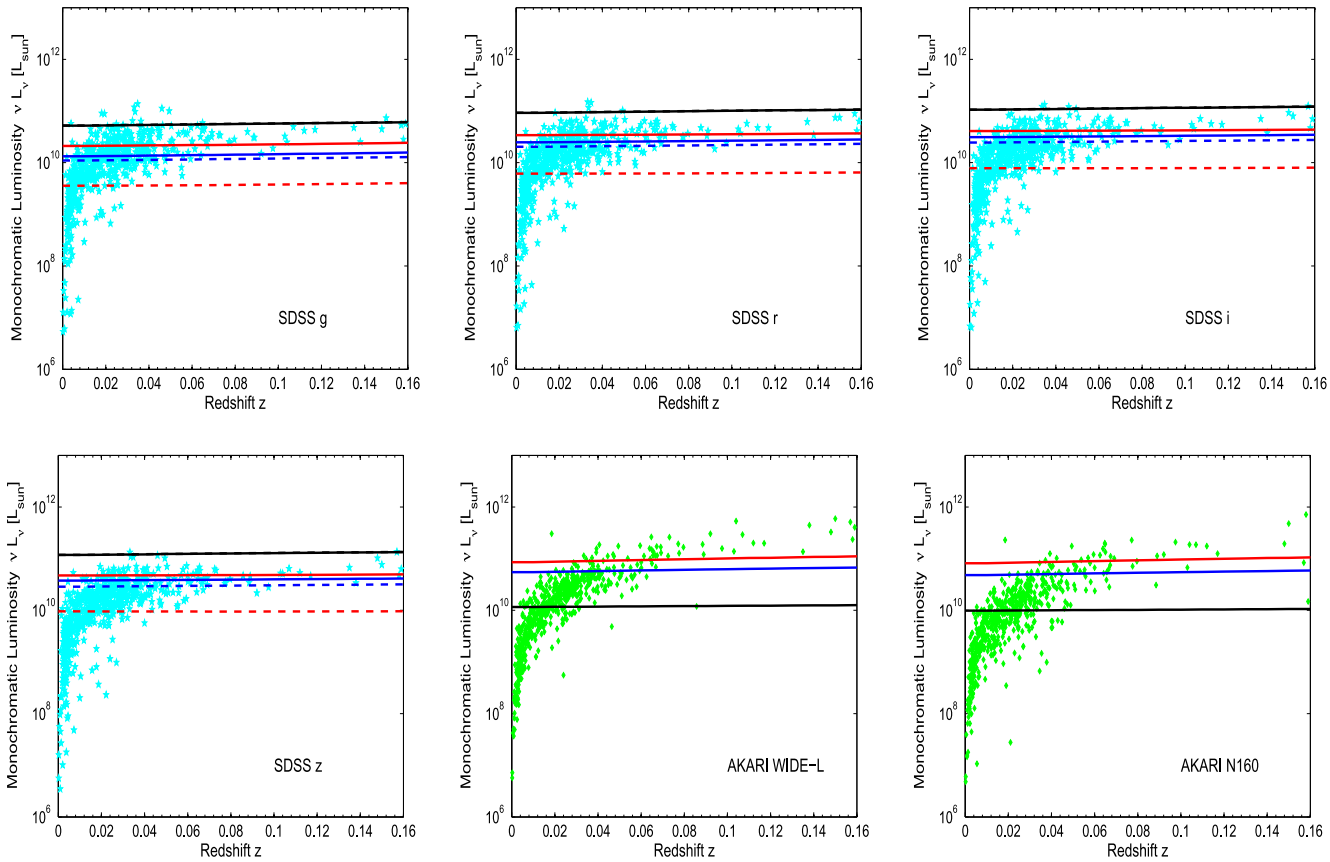

Figure 10. The same as in Fig. 9, but for the *g*, *r*, *i*, *z* passbands of SDSS and the AKARI passbands WIDE-L and N160 in the FIR.

do not include a proper description of the formation/destruction of dust as for instance recently developed by Dwek (1998, 2005) and Piovan et al. (2011a,b,c). Even if the dust content can be related to the metallicity of the galaxy, the relative proportions of the various components of the dust would require the detailed study of the evolution of the dusty environment and the complete information on the dust yields (Dwek 1998, 2005; Galliano, Dwek & Chanial 2005; Piovan et al. 2011a,b,c). This would lead to a better and more physically sound correlation between the composition of dust, the star formation activity and rate, and the chemical enrichment history of the galaxy itself. All this is missing in most galaxy models in which dust is considered. The problem may be particularly severe for high-metallicity environments. Secondly, the models for the disc galaxies with a central bulge need to be tested against SEDs of local galaxies of intermediate type going from *S*0 to *Sb*/*Sc*, trying to match some observational constraints, like the UV–optical average colours (Buzzoni 2002, 2005). Finally, many other physical ingredients can be improved and/or considered. Just to mention two of these, the extension of the SED to the radio range and the simulation of the nebular emission. Work is in progress to this aim.

Extensive tabulations of the SEDs, magnitudes, and colours of the SSPs and model galaxies are available from Cassarà upon request.

ACKNOWLEDGEMENTS

We are grateful to Alberto Buzzoni for fruitful discussions. LPC thanks Dario Maccagni for his help and support. This study makes use of data products from 2MASS, which is a joint project of the University of Massachusetts and the Infrared Processing and Analysis Centre/California Institute of Technology, founded by the National Aeronautics and Space Administration and the National Science Foundation. We would like to thank the anonymous referee whose comments improved the quality of the manuscript.

REFERENCES

Arimoto N., Jablonka P., 1991, A&A, 249, 374
Arimoto N., Yoshii Y., 1987, A&A, 173, 23
Bakes E. L. O., Tielens A. G. G. M., 1994, ApJ, 427, 822
Bertin G., Saglia R. P., Stiavelli M., 1992, ApJ, 384, 423
Bouwens R. J. et al., 2014, ApJ, 795, 126
Breitschwerdt D., Komossa S., 2000, AP&SS, 272, 3
Bressan A., Chiosi C., Fagotto F., 1994, ApJS, 94, 63
Bressan A., Silva L., Granato G. L., 2002, A&A, 392, 377
Bruzual A. G., Magris G., Calvet N., 1988, ApJ, 333, 673
Burkert A., Truran J. W., Hensler G., 1992, ApJ, 391, 651
Buta R., Mitra S., de Vaucouleurs G., Corwin H. G., Jr, 1994, AJ, 107, 118
Buzzoni A., 1995, in Buzzoni A., Renzini A., Serrano A., eds, ASP Conf. Ser. Vol. 86, Fresh Views of Elliptical Galaxies. Astron. Soc. Pac., San Francisco, p. 189
Buzzoni A., 2002, AJ, 123, 1188
Buzzoni A., 2005, MNRAS, 361, 725
Calzetti D., Heckman T. M., 1999, ApJ, 519, 27
Capak P. et al., 2007, ApJS, 172, 99
Carilli C. L. et al., 2001, ApJ, 555, 625
Carraro G., Ng Y. K., Portinari L., 1998, MNRAS, 296, 1045
Cassarà L. P., 2008, Master's thesis, Univ. Padova
Cassarà L. P., 2012, PhD thesis, Univ. Padova
Cassarà L. P., Piovan L., Weiss A., Salaris M., Chiosi C., 2013, MNRAS, 436, 2824
Chiosi C., 1980, A&A, 83, 206
Chiosi C., Carraro G., 2002, MNRAS, 335, 335
Chiosi C., Maeder A., 1986, ARA&A, 24, 329
Davidge T. J., 2001, AJ, 122, 1386
Desert F. X., Boulanger F., Shore S. N., 1986, A&A, 160, 295
Dickinson M. et al., 2004, ApJ, 600, L99
Draine B. T., 2003, ARA&A, 41, 241
Draine B. T., 2009, in Henning T., Grün E., Steinacker J., eds, ASP Conf. Ser. Vol. 414, Cosmic Dust - Near and Far. Astron. Soc. Pac., San Francisco, p. 453
Draine B. T., Lee H. M., 1984, ApJ, 285, 89
Draine B. T., Li A., 2001, ApJ, 551, 807
Draine B. T., Sutin B., 1987, ApJ, 320, 803
Dwek E., 1998, ApJ, 501, 643
Dwek E., 2005, in Popescu C. C., Tuffs R. J., eds, AIP Conf. Proc. Vol. 761, The Spectral Energy Distributions of Gas-Rich Galaxies: Confronting Models with Data. Am. Inst. Phys., New York, p. 103
Dwek E., Cherchneff I., 2011, ApJ, 727, 63
Dwek E., Galliano F., Jones A., 2009, in Henning T., Grün E., Steinacker J., eds, ASP Conf. Ser. Vol. 414, Cosmic Dust - Near and Far. Astron. Soc. Pac., San Francisco, p. 183
Fioc M., Rocca-Volmerange B., 1997, A&A, 326, 950
Froehlich H.-E., 1982, Astron. Nachr., 303, 97
Frogel J. A., 1988, ARA&A, 26, 51
Frogel J. A., 1999, AP&SS, 265, 303
Gall C., Andersen A. C., Hjorth J., 2011a, A&A, 528, A13
Gall C., Andersen A. C., Hjorth J., 2011b, A&A, 528, A14
Galliano F., Dwek E., Chanial P., 2005, Am. Astron. Soc. Meeting Abstracts, 207, #43.06
Galliano F., Dwek E., Chanial P., 2008, ApJ, 672, 214
Gavazzi G., Boselli A., Kennicutt R., 1991, AJ, 101, 1207
Geisler D., Friel E. D., 1992, AJ, 104, 128
Gibson B. K., Sánchez-Blázquez P., Courty S., Kawata D., 2007, in Emsellem E., Wozniak H., Massacrier G., Gonzalez J.-F., Devriendt J., Champavert N., eds, EAS Publ. Ser., Vol. 24, Chemodynamical Simulations of Elliptical Galaxies. Cambridge Univ. Press, Cambridge, p. 133
Goudfrooij P., Gorgas J., Jablonka P., 1999, AP&SS, 269, 109
Grassi T., Krstic P., Merlin E., Buonomo U., Piovan L., Chiosi C., 2011, A&A, 533, A123
Guhathakurta P., Draine B. T., 1989, ApJ, 345, 230
Hinshaw G. et al., 2009, ApJS, 180, 225
Im M., Casertano S., Griffiths R. E., Ratnatunga K. U., Tyson J. A., 1995, ApJ, 441, 494
Jablonka P., Arimoto N., Martin P., 1996, in Bender R., Davies R. L., eds, Proc. IAU Symp. 171, New Light on Galaxy Evolution. Kluwer, Dordrecht, p. 395
Jonsson P., Groves B. A., Cox T. J., 2010, MNRAS, 403, 17
Laor A., Draine B. T., 1993, ApJ, 402, 441
Larson R. B., 1976, MNRAS, 166, 585
Li A., Draine B. T., 2001, ApJ, 554, 778
Li A., Mayo Greenberg J., 2002, in Pirronello V., Krelowski J., eds, Solid State Astrochemistry. Kluwer, Dordrecht, p. 1
Madau P., Ferguson H. C., Dickinson M. E., Giavalisco M., Steidel C. C., Fruchter A., 1996, MNRAS, 283, 1388
Marigo P., Girardi L., Bressan A., Groenewegen M. A. T., Silva L., Granato G. L., 2008, A&A, 482, 883
Mathis J. S., 1990, ARA&A, 28, 37
Matteucci F., Greggio L., 1986, A&A, 154, 279
Mattila K., Lemke D., Haikala L. K., Laureijs R. J., Leger A., Lehtinen K., Leinert C., Mezger P. G., 1996, A&A, 315, L353
Merlin E., Chiosi C., 2007, A&A, 473, 733
Merlin E., Buonomo U., Grassi T., Piovan L., Chiosi C., 2010, A&A, 513, A36
Merlin E., Chiosi C., Piovan L., Grassi T., Buonomo U., Barbera F. L., 2012, MNRAS, 427, 1530
Michałowski M. J., Murphy E. J., Hjorth J., Watson D., Gall C., Dunlop J. S., 2010, A&A, 522, A15
Mobasher B. et al., 2007, ApJS, 172, 117
Narayanan D. et al., 2010, MNRAS, 407, 1701
Oesch P. A. et al., 2012, ApJ, 745, 110

Onaka T., Yamamura I., Tanabe T., Roellig T. L., Yuen L., 1996, PASJ, 48, L59
Origlia L., Valenti E., Rich R. M., 2005, MNRAS, 356, 1276
Pence W., 1976, ApJ, 203, 39
Piovan L., Tantalo R., Chiosi C., 2003, A&A, 408, 559
Piovan L., Tantalo R., Chiosi C., 2006a, MNRAS, 366, 923
Piovan L., Tantalo R., Chiosi C., 2006b, MNRAS, 370, 1454
Piovan L., Chiosi C., Merlin E., Grassi T., Tantalo R., Buonomo U., Cassarà L. P., 2011a, preprint (arXiv:1107.4541)
Piovan L., Chiosi C., Merlin E., Grassi T., Tantalo R., Buonomo U., Cassarà L. P., 2011b, preprint (arXiv:1107.4561)
Piovan L., Chiosi C., Merlin E., Grassi T., Tantalo R., Buonomo U., Cassarà L. P., 2011c, preprint (arXiv:1107.4567)
Pipino A., Fan X. L., Matteucci F., Calura F., Silva L., Granato G., Maiolino R., 2011, A&A, 525, A61
Popescu C. C., Tuffs R. J., Dopita M. A., Fischera J., Kylafis N. D., Madore B. F., 2011, A&A, 527, A109
Portinari L., Chiosi C., 1999, A&A, 350, 827
Portinari L., Chiosi C., 2000, A&A, 355, 929
Portinari L., Chiosi C., Bressan A., 1998, A&A, 334, 505
Puget J. L., Leger A., Boulanger F., 1985, A&A, 142, L19
Rich R. M., 1990, ApJ, 362, 604
Roberts M. S., Haynes M. P., 1994, ARA&A, 32, 115
Robson I., Priddey R. S., Isaak K. G., McMahon R. G., 2004, MNRAS, 351, L29
Rowan-Robinson M., 2012, in Tuffs R. J., Popescu C. C., eds, Proc. IAU Symp. 284, The Spectral Energy Distribution of Galaxies. Cambridge Univ. Press, Cambridge, p. 446
Sadler E. M., Rich R. M., Terndrup D. M., 1996, AJ, 112, 171
Saglia R. P., Bertin G., Stiavelli M., 1992, ApJ, 384, 433
Saito M., 1979a, PASJ, 31, 181
Saito M., 1979b, PASJ, 31, 193
Schmidt M., 1959, ApJ, 129, 243
Scoville N. et al., 2007, ApJS, 172, 1
Sellgren K., Werner M. W., Dinerstein H. L., 1983, ApJ, 271, L13
Shapley A. E., Steidel C. C., Adelberger K. L., Dickinson M., Giavalisco M., Pettini M., 2001, ApJ, 562, 95
Silva L., 1999, PhD thesis, SISSA
Silva L., Granato G. L., Bressan A., Danese L., 1998, ApJ, 509, 103
Spitoni E., Matteucci F., Marcon-Uchida M. M., 2013, A&A, 551, A123
Springel V., Di Matteo T., Hernquist L., 2005, ApJ, 620, L79
Stanway E. R., Bunker A. J., McMahon R. G., 2003, MNRAS, 342, 439
Steidel C. C., Adelberger K. L., Giavalisco M., Dickinson M., Pettini M., 1999, ApJ, 519, 1
Takagi T., Vansevicius V., Arimoto N., 2003, PASJ, 55, 385
Takeuchi T. T., Buat V., Heinis S., Giovannoli E., Yuan F.-T., Iglesias-Páramo J., Murata K. L., Burgarella D., 2010, A&A, 514, A4
Talbot R. J., Arnett W. D., 1971, ApJ, 170, 409
Tanaka M., Matsumoto T., Murakami H., Kawada M., Noda M., Matsuura S., 1996, PASJ, 48, L53
Tantalo R., Chiosi C., Bressan A., Fagotto F., 1996, A&A, 311, 361
Tantalo R., Chiosi C., Bressan A., Marigo P., Portinari L., 1998, A&A, 335, 823
Tantalo R., Chinellato S., Merlin E., Piovan L., Chiosi C., 2010, A&A, 518, A43
Tiede G. P., Frogel J. A., Terndrup D. M., 1995, BAAS, 27, 884
Wang R., Carilli C. L., Neri R., Walter F., Bertoldi F., Cox P., 2009, in Wang W., Yang Z., Luo Z., Chen Z., eds, ASP Conf. Ser., Vol. 408, The Starburst-AGN Connection. Astron. Soc. Pac., San Francisco, p. 452
Weingartner J. C., Draine B. T., 2001a, ApJS, 134, 263
Weingartner J. C., Draine B. T., 2001b, ApJ, 548, 296
Weiss A., Ferguson J. W., 2009, A&A, 508, 1343
Whitford A. E., Rich R. M., 1983, ApJ, 274, 723
Wise M. W., Silva D. R., 1996, ApJ, 461, 155
Witt A. N., Thronson H. A., Capuano J. M., 1992, ApJ, 393, 611
Yamasawa D., Habe A., Kozasa T., Nozawa T., Hirashita H., Umeda H., Nomoto K., 2011, ApJ, 735, 44
Yi S. K., Yoon S.-J., 2004, AP&SS, 291, 205
Zheng W. et al., 2012, Nature, 489, 406
Zhukovska S., Gail H.-P., Trieloff M., 2008, A&A, 479, 453
Zoccali M. et al., 2003, A&A, 399, 931

This paper has been typeset from a TEX/LATEX file prepared by the author.